Constraints on the Origin and Evolution of Magmas in the Payún Matrú Volcanic Field, Quaternary Andean Back-arc of Western Argentina

I. R. HERNANDO[1]*, E. ARAGÓN[1], R. FREI[2], P. D. GONZÁLEZ[3] AND W. SPAKMAN[4]

[1]CENTRO DE INVESTIGACIONES GEOLÓGICAS, UNIVERSIDAD NACIONAL DE LA PLATA–CONICET, 1 NO. 644, B1900TAC, LA PLATA, ARGENTINA

[2]DEPARTMENT OF GEOGRAPHY AND GEOLOGY & NORDIC CENTRE FOR EARTH EVOLUTION (NORDCEE), UNIVERSITY OF COPENHAGEN, ØSTER VOLDGADE 10, DK-1350 COPENHAGEN, DENMARK

[3]INSTITUTO DE INVESTIGACIÓN EN PALEOBIOLOGÍA Y GEOLOGÍA, UNIVERSIDAD NACIONAL DE RÍO NEGRO, ISIDRO LOBO 516, CP 8332, GENERAL ROCA, ARGENTINA

[4]VENING MEINESZ RESEARCH SCHOOL OF GEODYNAMICS, FACULTY OF EARTH SCIENCES, UTRECHT UNIVERSITY, BUDAPESTLAAN 4, 3584DC, UTRECHT, NETHERLANDS

The Payún Matrú Volcanic Field (Pleistocene–Holocene) is located in the Andean back-arc of the Southern Volcanic Zone, western Argentina, and is contemporaneous with the Andean volcanic arc at the same latitude. It includes two polygenetic, mostly trachytic volcanoes: Payún Matrú (with a summit caldera 8 km wide) and Payún Liso (a smaller stratovolcano). The volcanic field includes about 200 scoria cones and alkali basaltic and trachybasaltic lava flows, forming two basaltic fields around Payún Matrú. New ^{40}Ar–^{39}Ar ages extend the activity of Payún Matrú up to 700 ka. The major and trace element and Sr–Nd isotopic compositions of the basaltic lavas and Payún Matrú rocks indicate that the trachytes of Payún Matrú are the result of fractional crystallization of basaltic parent magmas without significant upper crustal contamination, and that the basalts have a geochemical similarity to ocean island basalt (La/Nb = 0·8–1·5, La/Ba = 0·05–0·08). The Sr–Nd isotopic compositions of the basaltic to trachytic rocks range between 0·703813 and 0·703841 ($^{87}Sr/^{86}Sr$) and 0·512743 and 0·512834 ($^{143}Nd/^{144}Nd$). Mass-balance and Rayleigh fractionation models support the proposed origin of the trachytes, and an assimilation–fractional crystallization model indicates a low degree of upper crustal contamination in the youngest trachytes. Magnesium numbers (45–55) and contents of Ni (<20–90 ppm) and Cr (30–180 ppm) in the lavas in the basaltic fields indicate that these are not primary magmas. The data also suggest that the basaltic lavas originated in the asthenospheric mantle, probably within the spinel stability field and beneath an attenuated continental lithosphere in the back-arc area. The lack of a slab-fluid signature in the Payún Matrú Volcanic Field rocks, along with unpublished and published geophysical results (mantle tomography and electrical conductivity anomalies) suggest that magmas were generated by decompression-induced melting of upwelling mantle.

KEY WORDS: *alkali basalts; Andes back-arc; intra-plate magmatism; trachyte*

*Corresponding author. Telephone: 0054 221 4215677. Fax: 0054 221 4827560. E-mail: ihernando@cig.museo.unlp.edu.ar

INTRODUCTION

In mid west Argentina, at the latitude of the Southern Volcanic Zone of the Andes, there has been abundant volcanic activity in the back-arc area from Pliocene to Holocene times. This volcanism consists mainly of alkali basalts, and was termed the Payenia Basaltic Province, or Payenia by Polanski (1954) (Fig. 1). Although volcanism in the Andes is widespread along the arc axis, the volcanism in the back-arc zone is not as well developed, with the exception of Payenia, which represents the largest basaltic province of South America in this time period (Folguera et al., 2009). The Payún Matrú Volcanic Field (PMVF) is one of the major volcanic fields within Payenia. Its age is Pleistocene–Holocene and it includes the majority of the most recent Holocene volcanic activity in Payenia.

Although there have been a number of studies on the origin of the Payenia volcanism (Bermúdez & Delpino, 1989; Bermúdez et al., 1993; Kay et al., 2006a; Llambías et al., 2010; Ramos & Folguera, 2011; Gudnason et al., 2012), the particular history and petrogenesis of the PMVF has remained poorly studied (Llambías, 1966; Hernando et al., 2012). Here we present whole-rock chemical and Sr–Nd isotope data and ^{40}Ar–^{39}Ar ages for the Payún Matrú Volcanic Field with the aim of elucidating the origin and evolution of the magmas, and how the Payún Matrú volcano and surrounding basaltic rocks are related.

GEOLOGICAL SETTING

Payenia (34–38°S) (Polanski, 1954) is located in the back-arc of the Southern Volcanic Zone of the Andes (Fig. 1); its age is Pliocene–Holocene (5 Ma to historical) (Bermúdez & Delpino, 1989; Inbar & Risso, 2001; Germa et al., 2010; Llambías et al., 2010; Gudnason et al., 2012; Españon et al., 2013). The volcanism in Payenia is principally characterized by eruptions of alkali basalts with an intraplate geochemical affinity (Stern et al., 1990; Bermúdez et al., 1993; Kay, 2002; Kay et al., 2004, 2006a), and it is contemporaneous with the activity in the volcanic arc at the same latitude, located along the Argentina–Chile frontier (Fig. 1). Payenia is located ∼500 km away from the Chilean segment of the Perú–Chile trench and 150–300 km east of the volcanic arc axis; it covers an area of about 16 000 km^2 (Bermúdez et al., 1993). This basaltic province includes the
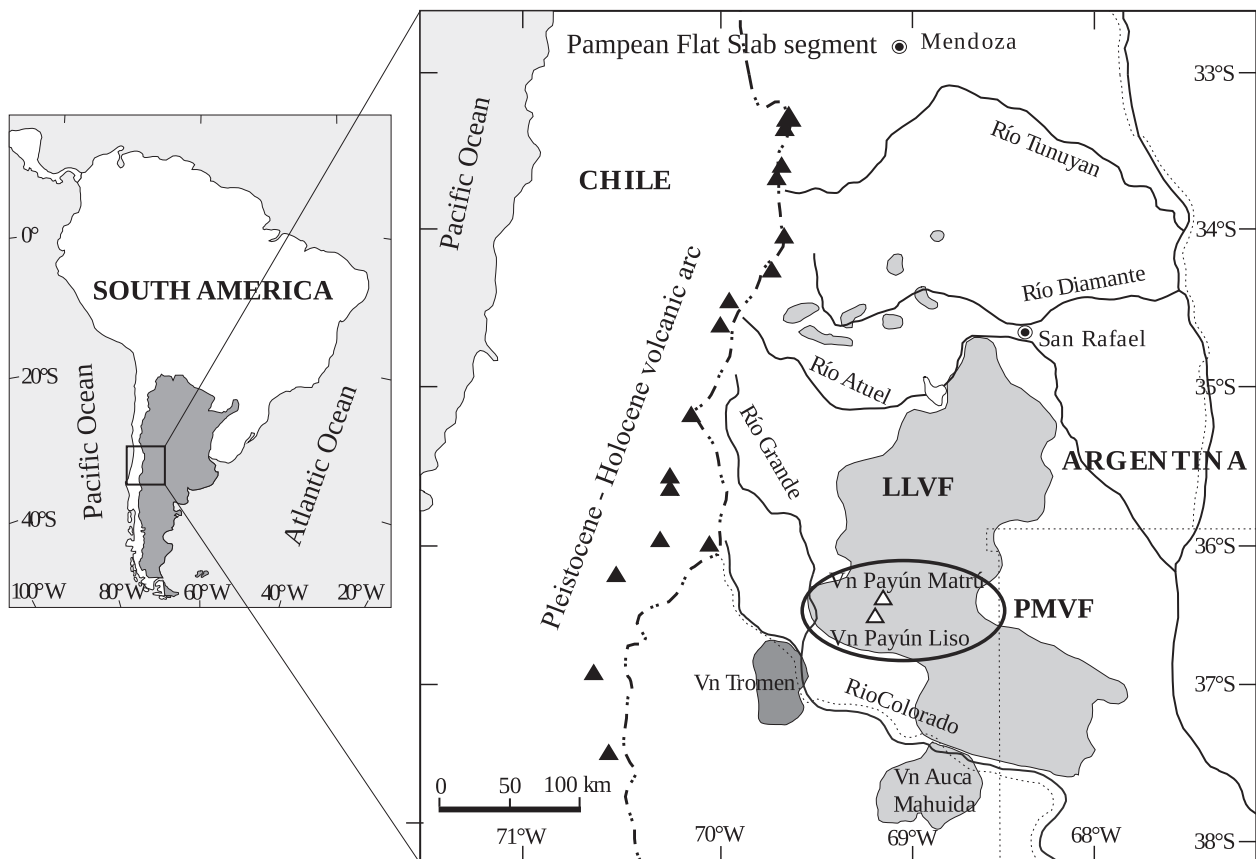

Fig. 1. Location map of the Payenia Basaltic Province (light gray) in the back-arc of the Southern Volcanic Zone of the Andes and the Pleistocene–Holocene volcanic arc (black triangles). The Tromen volcanic complex (dark gray) is not generally considered as part of Payenia. The oval indicates the location of the Payún Matrú Volcanic Field (PMVF). LLVF, Llancanelo Volcanic Field.

PMVF (36–37°S, 68°30′–69°40′W), with an area of 5200 km[2] (Bermúdez *et al.*, 1993), the Llancanelo Volcanic Field (LLVF), and some dispersed monogenic centers north of the LLVF (Fig. 1; Bermúdez & Delpino, 1989; Bermúdez *et al.*, 1993; Llambías *et al.*, 2010).

During Miocene times, between 19 and 4 Ma, volcanic activity with a subduction-related geochemical affinity took place in the present back-arc (Kay *et al.*, 2006*b*; Ramos & Kay, 2006). In this period a compressional tectonic regime formed the Malargüe fold and thrust belt, along with syn-orogenic sedimentation in the orogenic front (Ramos & Folguera, 2005; Ramos & Kay, 2006). These features were interpreted as a period of flat subduction at the latitude of Payenia, which peaked in the late Miocene (8–5 Ma) (Kay *et al.*, 2006*a*). Subsequently, an extensional tectonic regime and normal subduction occurred during Pliocene–Holocene times, owing to the steepening of the subducting Nazca plate (Kay *et al.*, 2006*a*; Ramos & Kay, 2006; Gudnason *et al.*, 2012). During this period the extensive volcanism of Payenia occurred in the Andean back-arc region. The youngest Holocene volcanic activity is restricted to the PMVF, Tromen volcano, and a few monogenetic centers in northern Payenia (Llambías *et al.*, 2010).

The alkali basaltic magmatism in Payenia has been suggested to be the result of low-degree partial melting of an enriched mantle source (Kay, 2002; Kay *et al.*, 2004) with garnet as the Al-bearing phase (Bertotto *et al.*, 2009).

Payún Matrú Volcanic Field

The PMVF exhibits two contemporaneous and contrasting styles of volcanism. It includes two polygenetic volcanoes, Payún Matrú and Payún Liso, and two basaltic fields located east and west of Payún Matrú (Fig. 2). The basaltic eruptive centres and Payún Matrú volcano are distributed along a relatively narrow east–west axis, with the polygenetic volcano in the centre, surrounded by an eastern and a western basaltic field (Fig. 2; Hernando *et al.*, 2012). These two basaltic fields contain more than 200 scoria cones and numerous lava flows. The Payún Matrú volcano is a shield-shaped edifice with a summit caldera 8 km wide (Llambías, 1966; Hernando *et al.*, 2012) whereas Payún Liso is a typical stratovolcano (Fig. 2a and b). The Payún Matrú caldera provides strong evidence for the presence of a shallow magma chamber (Lipman, 2000; Parfitt & Wilson, 2008), at least during the syn- and post-caldera stages. This contrasts with the relatively deep origin and probable storage zone of the basaltic magmas.

The age of the PMVF was previously estimated to be Pleistocene–Holocene (Llambías, 1966; González Díaz, 1972), and recently constrained to the last 300 ka (Germa *et al.*, 2010). Five ^{40}Ar–^{39}Ar ages determined for Payún Liso lavas indicate a Pleistocene age, between 320 ± 20 and 261 ± 4 ka (Germa *et al.*, 2010; Gudnason *et al.*, 2012), whereas the ages of Payún Matrú lavas range from 168 ± 4 to 7 ± 1 ka (Germa *et al.*, 2010). The ^{40}Ar–^{39}Ar ages determined for basaltic groundmass of lavas in the western basaltic field range from 320 ± 50 ka to <7 ka (Germa *et al.*, 2010; Gudnason *et al.*, 2012). Cosmogenic ^{21}Ne and ^{3}He mean ages of bombs and lavas from the western basaltic field range from $48 \cdot 2 \pm 1 \cdot 1$ ka to $2 \cdot 4 \pm 2 \cdot 1$ ka (Españon *et al.*, 2013), and exposure mean age determined from cosmogenic ^{3}He in basaltic lavas along the Rio Grande is 41 ± 1 ka (Marchetti *et al.*, 2006).

The stratigraphy of the PMVF was first outlined by Groeber (1946), Llambías (1966), González Díaz (1972) and Bermúdez *et al.* (1993), and it was later modified by Hernando *et al.* (2012), whose stratigraphy is used in this study. A detailed geological map of the PMVF has also been presented by Hernando *et al.* (2012). The PMVF is divided into a pre-caldera, a syn-caldera and a post-caldera stage (Hernando *et al.*, 2012) on the basis of a unique ignimbrite sheet associated with the formation of the Payún Matrú caldera: the Portezuelo Ignimbrite (Llambías, 1966). The basaltic fields are divided into three units: Pre-caldera Basalts, Post-caldera Basalts I and Post-caldera Basalts II (Hernando *et al.*, 2012). The Payún Matrú volcano consists of four units: Pre-caldera Trachytes, Portezuelo Ignimbrite, Post-caldera Trachyandesites, and Post-caldera Trachytes. This latest unit has been further subdivided into three lithofacies, interspersed in time: Blocky Trachytes (represented by blocky lava flows), Pumiceous Cones (proximal pyroclastic fall deposits) and Vitreous Trachytes (vitrophyric domes and lava flows) (Hernando *et al.*, 2012). The Payún Liso volcano belongs to the pre-caldera stage of the volcanic field and, because it has not been studied in detail, it is grouped in a single unit here.

SAMPLING AND ANALYTICAL PROCEDURES

Samples were collected mostly from Payún Matrú volcano and the eastern and western basaltic fields, with a minor selection of Payún Liso rocks. Fifty-six fresh samples were crushed and milled at the Centro de Investigaciones Geológicas (CONICET–UNLP, Argentina) using a mill with tungsten carbide rings. As this procedure may lead to W and Co contamination, these elements were not used in the interpretations. The whole-rock major and trace elements were later analyzed at the Actlabs Ltd. Laboratories in Ontario, Canada [using lithium metaborate–tetraborate carbonate fusion inductively coupled plasma-mass spectrometry (ICP-MS) methods]. The fused sample was diluted and analyzed by Perkin Elmer Sciex ELAN 6000, 6100 or 9000 ICP-MS system. In each group of samples three blanks and five controls were analyzed, and duplicates were fused and analyzed every 15 samples and the instrument was recalibrated every 40 samples.
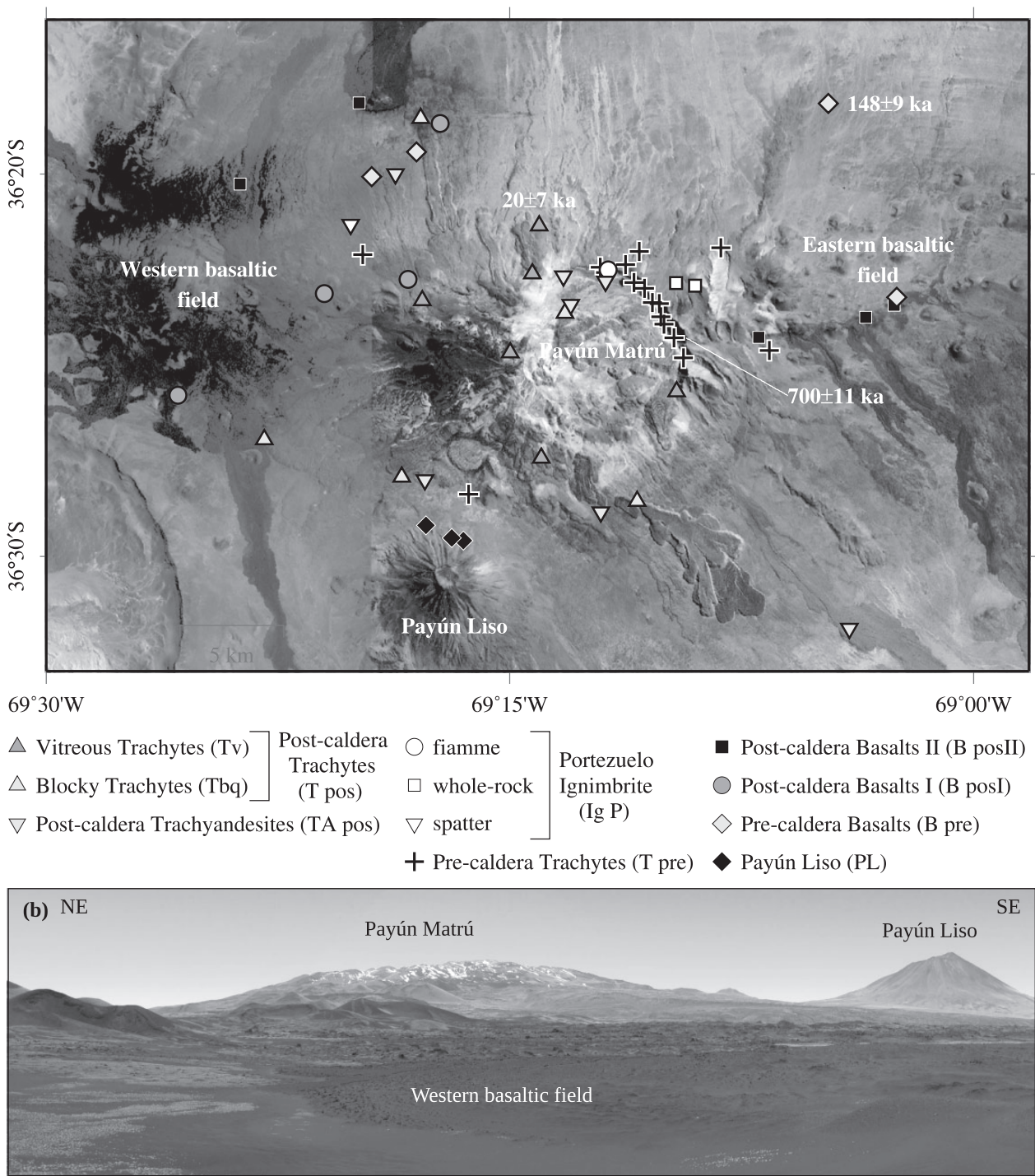
Fig. 2. (a) LANDSAT 7 satellite image of the PMVF (NASA Landsat Program, 2000-200l, Landsat ETM+ scenes p23lr085 7x200003l7 and p232r085 7x200l0207, orthorectified, GLCF), showing the location of the samples analyzed. The Payun Matru caldera is located in the middle of an east-west zone with maximum concentration of scoria cones. (b) Photograph of the PMVF, looking east from the western basaltic field.

In the case of the Portezuelo Ignimbrite, the lithic clasts content is low enough to make feasible hand picking extraction of the larger lithic fragments before whole-rock analysis, to minimize lithic clast contamination. In the case where fiamme were larger, a chemical analysis was obtained for a fiamme sample for comparison with the whole-rock, as fiamme represent the most reliable magma composition, without contamination or crystal

concentrations. A subset (only major elements) of these 56 samples was reported by Hernando *et al.* (2012). Fifteen of the samples analyzed for their whole-rock geochemistry were also analyzed for $^{87}Sr/^{86}Sr$ and $^{143}Nd/^{144}Nd$ at the University of Copenhagen, Denmark, following the method and analytical techniques described by Kalsbeek & Frei (2006).

Two lavas from Payún Matrú volcano and one lava from the eastern basaltic field were selected for $^{40}Ar-^{39}Ar$ dating. In addition, one sample of fiamme from the Portezuelo Ignimbrite was selected for $^{40}Ar-^{39}Ar$ dating; however, it was not possible to determine its age owing to the low Ar content of the feldspars. The $^{40}Ar-^{39}Ar$ dating was performed at the University of Wisconsin–Madison (USA). The lava from the eastern basaltic field was incrementally heated following the methods of Jicha *et al.* (2012), and laser total fusion experiments were performed on feldspars from the two Payún Matrú lavas.

Cross-sections and maps from a global tomographic model at the latitude of the Southern Andes were made after Bijwaard *et al.* (1998) and Bijwaard & Spakman (2000), based on perturbations in P-wave velocities in the mantle, as described by Amaru (2007). Sensitivity test results from seven synthetic wave-speed block models are shown in Electronic Appendix 1 (all supplementary material is available for downloading at http://www.petrology.oxfordjournals.org).

RESULTS
Petrography
The petrography of PMVF rocks was described in detail by Hernando *et al.* (2012); here we summarize the main petrographic characteristics of the PMVF rocks (Table 1).

Pre-caldera Trachytes
This unit is the most diverse. It ranges from trachytes with alkali feldspars (5–18%) and without plagioclase phenocrysts, to basaltic trachyandesites with plagioclase (1–20%) and no alkali feldspar phenocrysts. Clinopyroxene is the most common mafic phenocryst (<5%), followed by olivine (<5%), which is not always present. Other mafic phases (observed in fewer lavas) are biotite (<4%) and amphibole (<3%). Opaque minerals are always present and apatite is a common accessory phase. Groundmasses are mostly pilotaxitic, but are intergranular in some intermediate lavas. There are scarce

Table 1: Summary of the main petrographic characteristics of the PMVF units

	Pre-caldera Trachytes	Portezuelo Ignimbrite	Post-caldera Trachyandesites	Post-caldera Trachytes	Pre- and Post-caldera Basalts I–II
Rock	Trachytes ≫ trachyandesites > basaltic trachyandesites	Trachytes	Basaltic trachyandesites > trachyandesites	Trachytes ≫ rhyolites	Basalts and trachybasalts
Alkali feldspar	From 5–18% in the most silicic samples (and without plagioclase) to absent in intermediate samples	<5%	Absent	5–20%	Absent
Plagioclase	From 1–20% to absent in the most silicic samples	4–16%	10–22%	Generally absent	<1% up to 10% in few samples, absent in some lavas
Olivine	<5%, not always present	<3%	2–5%	<3%, not always present in the Blocky Trachytes lithofacies	1–5%
Clinopyroxene	<5%, the most frequent mafic mineral	<3%	2–5%	<4%	1–5%; absent in some lavas
Amphibole	<3%, present in few lavas	Absent	Present in only one lava, <1%	Absent	Absent
Biotite	<4%, present in few lavas	<3%	Absent	<2%, in some lavas	Absent
Mixing or mingling textures	Common mixing textures, rare mingling textures	Absent	Abundant mixing textures, rare minglingtextures	Absent	Rare mingling textures

trachytic pre-caldera ignimbrites, with a high degree of welding and eutaxitic texture.

Some lavas have abundant mineralogical textures indicative of simple or partial dissolution of feldspar phenocrysts (such as dusty and coarse sieve textures and rounded crystals), along with non-dissolved phenocrysts (Fig. 3a). Mafic minerals in these lavas sometimes have rounded corners, commonly observed in clinopyroxene; biotite also shows replacement by anhydrous minerals. In a few lavas two texturally different groundmass domains with a fluid–fluid relationship are observed (Fig. 3b). The repeated presence of dissolution and/or replacement textures and also (in fewer cases) the presence of different groundmass domains suggests that mixing or mingling of magmas was a recurring process in the pre-caldera stage of Payún Matrú (Hernando et al., 2012).

Portezuelo Ignimbrite

Although the petrographic characteristics of the ignimbrite vary vertically and laterally owing to variations in the degree of welding and its components, the crystal content and its characteristics remain relatively constant. Considering the crystal content of the whole-rock, plagioclase crystals (4–16%) predominate over alkali feldspar (<5%). These crystals mostly suggest equilibrium conditions during growth, although there are minor proportions of sieved crystals (Fig. 3c). The mafic minerals present are olivine, clinopyroxene and biotite (<3% each), plus opaque minerals and apatite as an accessory phase. Fiamme and pumice show the same mineral assemblage as the matrix, although with a smaller percentage of crystals than the latter, generally below 10% (Fig. 3c). The glass in these juvenile clasts is frequently, but not always, recrystallized (Fig. 3c).

Post-caldera Trachyandesites

These are porphyritic lavas with phenocrysts of plagioclase (10–22%), olivine (2–5%) and clinopyroxene (2–5%) in an intergranular to pilotaxic groundmass. Amphibole is rare (<1%) and it is present in only one lava flow. All lavas of this unit, with only one exception, include both unsieved and sieved plagioclase, with dusty and coarse sieve textures (Fig. 3d). The only intra-caldera lava flow of this unit shows evidence of mingling between trachytic and basaltic trachyandesitic magma, in which the latter constitutes the majority of the flow (Hernando et al., 2012).

Post-caldera Trachytes

These are porphyritic lavas and pumice deposits with phenocrysts of alkali feldspar (5–20%), olivine (<3%, not always present in Blocky Trachytes), clinopyroxene (<4%), and sometimes biotite (<2%), plus opaque minerals and accessory apatite. The Vitreous Trachytes lavas are vitrophyres (Fig. 3e), whereas the Blocky Trachytes are holocrystalline with a pilotaxic groundmass.

Pre-caldera and Post-caldera I and II Basalts

The majority of these lavas are porphyritic, although a few are aphyric, with an intergranular groundmass. The phenocrysts are olivine (1–5%), plagioclase (<1% up to 10% in a few cases), and clinopyroxene (<1% up to 5%). Olivine is always present, whereas plagioclase is absent in a few lavas and, more commonly, clinopyroxene phenocrysts are absent (Fig. 3f).

^{40}Ar–^{39}Ar ages

The pre-caldera sample of Payún Matrú selected for dating was collected in the lower zone of the eastern profile exposed by the caldera collapse (Fig. 2a). It is a trachytic lava with fresh alkali feldspars phenocrysts. The ^{40}Ar–^{39}Ar age determined is $700·6 \pm 10·6$ ka (Table 2). The post-caldera lava dated belongs to the Vitreous Trachytes lithofacies, and it is located in the northern rim of the caldera (Fig. 2a). Its age is $20·2 \pm 6·5$ ka (Table 2), supporting the interrelation in time with the lithofacies of the Post-caldera Trachytes unit [three ages of lavas of Blocky Trachytes determined by Germa et al. (2010) range between 26 ± 2 and 7 ± 1 ka]. The eruption age of the Pre-caldera Basalts flow in the eastern basaltic field (Fig. 2a) has a weighted mean plateau age of $148·4 \pm 8·7$ ka (Fig. 4). Although it was not possible to determine the age of the Portezuelo Ignimbrite, its eruption is constrained to between 148 and 82 ka, according to ages presented by Germa et al. (2010) and this study.

Major elements

Representative major and trace element and isotopic data for the PMVF rocks are given in Table 3 (the full dataset is given in the Supplementry Data Electronic Appendix 2). Sample locations are shown in Fig. 2a. The selected analyzed samples are fresh [i.e. without altered phenocrysts and groundmass (with the exception of olivine partly altered to iddingsite in some samples)] and with loss on ignition (LOI) values mostly below 1 wt % and rarely between 1 and 2 wt % (Table 3). In the case of the Portezuelo Ignimbrite, there is a moderate amount of vapour-phase crystallization in whole-rock samples PM 24, PM 26 and PM 43, although the crystals in the fiamme and matrix are unaltered. Post-eruptive alkali alteration by devitrification of glass in the presence of alkali-rich solutions may result in important changes in the alkalis, Al_2O_3, SiO_2 and H_2O contents and, in some cases, in other trace elements such as the rare earth elements (REE) (Lofgren, 1970; Weaver et al., 1990). Glass is present in samples of the Portezuelo Ignimbrite and Vitreous Trachytes. The analyzed samples of the Vitreous Trachytes lithofacies correspond to glass without devitrification (except for sample PMC 49) and without a perlitic texture; a result of hydration (Fig. 3e). The alkalis and REE contents of these rocks are similar to those of the holocrystalline Blocky Trachytes lithofacies, and LOI contents are
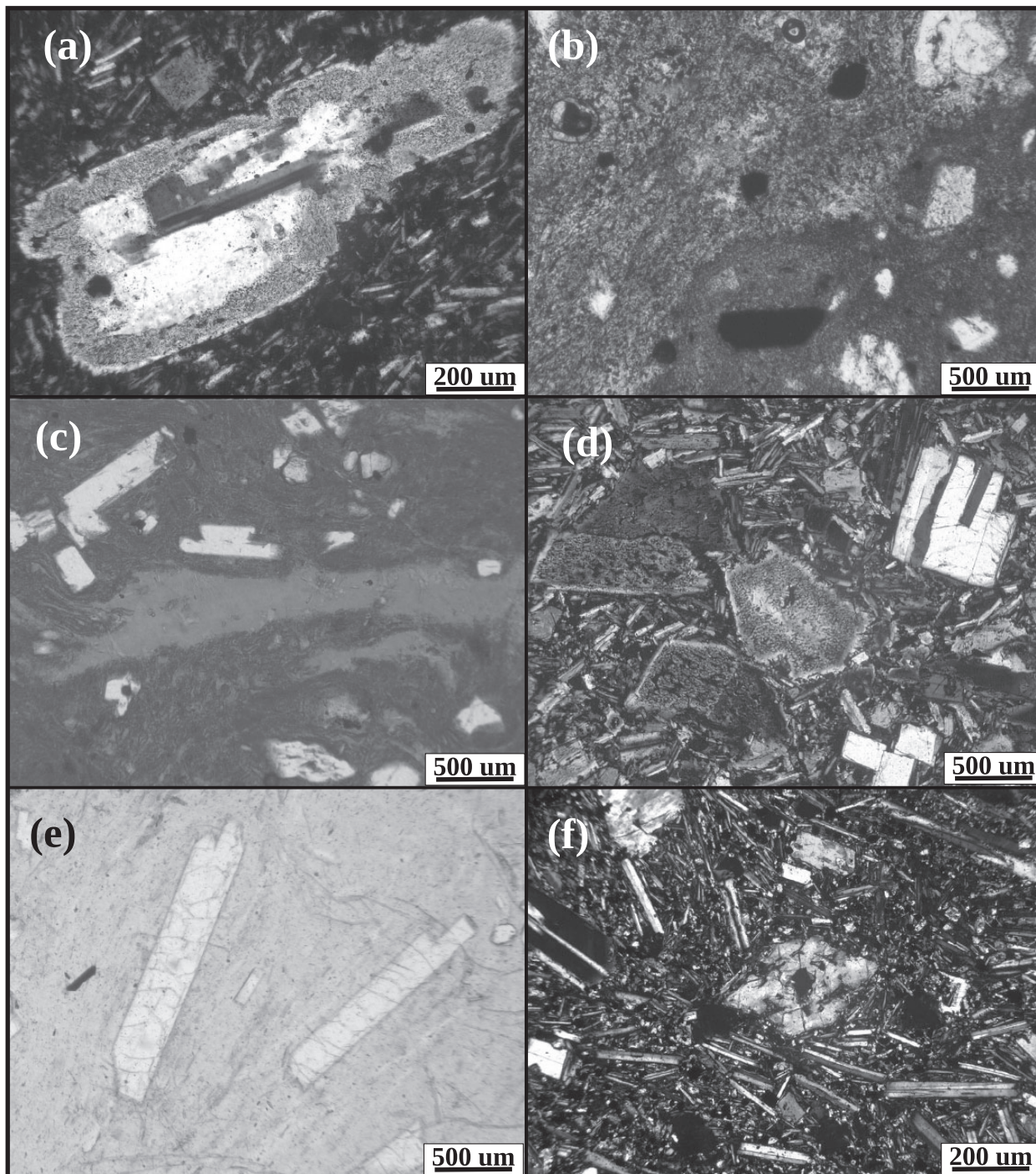
Fig. 3. Photomicrographs of PMVF rocks. (a) Dusty and rounded plagioclase phenocryst in a Pre-caldera Trachytes lava. (b) Two different groundmass domains in a trachyte lava of the pre-caldera stage. (c) Highly welded zone of the Portezuelo Ignimbrite in its most proximal section, with weakly recrystallized, glassy fiamme. (d) Post-caldera Trachyandesites lavas, showing non-sieved and sieved plagioclase phenocrysts. (e) Vitreous Trachytes lithofacies of the Post-caldera Trachytes unit. (f) Skeletal olivines in a basaltic lava of the Pre-caldera Basalts unit.

Table 2: Results of $^{40}Ar-^{39}Ar$ dating of three PMVF lavas

Sample	Lat. (°S)	Long. (°W)	Material	K/Ca total	Total fusion age (ka) ± 2σ	$^{40}Ar/^{36}Ar_i$ ± 2σ	MSWD	Isochron Age (ka) ± 2σ	n	$^{39}Ar\%$	MSWD	Weighted mean Age (ka) ± 2σ
Furnace incremental heating												
PY 5	36·30256	69·07819	groundmass	0·23	147·2 ± 14·5	296·2 ± 3·1	0·77	141·5 ± 50·7	7 of 9	95·4	0·67	153·5 ± 14·6
			groundmass	0·28	147·1 ± 12·1	295·9 ± 2·4	1·29	139·8 ± 34·9	9 of 9	100·0	1·14	145·4 ± 11·2
							Weighted mean plateau age from two experiments:					148·4 ± 8·7
Laser total fusion												
PMB12	36·35600	69·23420	sanidine	9·08		299·2 ± 24·0	0·94	17·8 ± 6·9	22 of 22	100·0	0·90	20·2 ± 6·5
PMD 60	36·35483	69·16155	anorthoclase	17·86		295·1 ± 4·2	0·44	701·8 ± 16·4	20 of 20	100·0	0·42	700·6 ± 10·6

J-value calculated relative to 28·201 Ma for the Fish Canyon sanidine. Sample PY 5, Pre-caldera Basalts unit; sample PMB 12, Vitreous Trachytes lithofacies (Post-caldera Trachytes unit); sample PMD 60, Pre-caldera Trachytes unit.
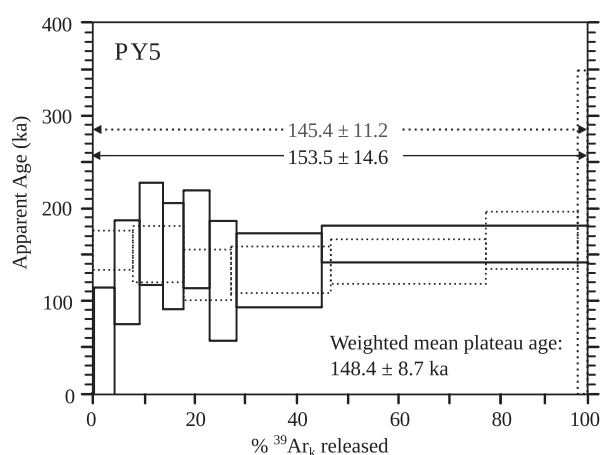

Fig. 4. $^{40}Ar-^{39}Ar$ plateau ages of groundmass separate from sample PY 5, Pre-caldera Basalts unit. Seven of nine steps were used for determination for the 145·4 ± 11·2 ka plateau age, and nine of nine for the 153·5 ± 14·6 ka plateau age.

low (below 1 wt %, except for PMC 49 with 1·18 wt % LOI). There is no clear correlation between LOI and any of the REE in these rocks (r^2 up to 0·46). Therefore, the Vitreous Trachytes lithofacies does not seem to show a significant post-eruptive alkali alteration or REE loss. In the case of the Portezuelo Ignimbrite, although the alkali contents seem to be unaffected, the REE in whole-rock samples PM 24, PM 26 and PM 43 differ significantly from those in the other samples, and therefore they are not considered in the data discussion.

The rocks of the PMVF belong to a transitional alkaline series, ranging from basalts to trachytes transitional to rhyolites (Fig. 5; Hernando *et al.*, 2012). Lavas in the eastern and western basaltic fields are basalts and trachybasalts, with silica contents between 46·7 and 50 wt %, on an

anhydrous basis. They have normative nepheline (<5 wt %), olivine (5–10 wt %), and diopside (13–20 wt %) and therefore are classified as alkali olivine basalts (Thompson, 1984). All Post-caldera Basalts II lavas are trachybasalts, whereas the basaltic lavas with the lowest silica and alkali contents belong to the Pre-caldera Basalts unit (Fig. 5). Continental alkali basalts, which include basalts and trachybasalts, can be divided into potassic and sodic types, according to their K_2O/Na_2O ratios (Farmer, 2003). The basalts and trachybasalts of the PMVF are clearly sodic (K_2O/Na_2O between 0·28 and 0·44), which is the most common type of continental alkali basalt (Farmer, 2003).

Lavas and pyroclastic rocks of Payún Matrú volcano are mostly trachytic, with trachyandesites and basaltic trachyandesites in minor proportions; basalts are absent. The Pre-caldera Trachytes unit is the most diverse (although it is mainly trachytic), with silica contents between 53·4 and 68 wt %, and ($Na_2O + K_2O$) between 7·6 and 11·3 wt %. Whole-rock, fiamme and spatter clast analyses from the Portezuelo Ignimbrite are all trachytic (62·8–65·3 wt % SiO_2, 9·9–11·1 wt % alkalis). The first post-caldera lavas erupted in Payún Matrú, represented by the Post-caldera Trachyandesites unit, indicate a shift to less evolved compositions (53·1–60·5 wt % SiO_2, 7·1–9·8 wt % alkalis). The only trachytic sample of this unit (sample PM 13) belongs to a restricted sector of the intra-caldera lava flow, which is mainly of basaltic trachyandesitic composition, and shows evidence of mingling between basaltic trachyandesitic and trachytic magmas (Hernando *et al.*, 2012). After the eruptions of these lavas, there was a shift to trachytic compositions. The Post-caldera Trachytes (along with a few Pre-caldera Trachytes) are the most silicic rocks in the volcanic field, and show a relatively narrow range in composition (67·6–69·6 wt % SiO_2, and 10·9–11·5 wt %

Table 3: Whole-rock major and trace element compositions of PMVF rocks

Unit:	Vitreous Trachytes (T pos)		Blocky Trachytes		Post-caldera Trachyandesites (T pos)				Portezuelo Ignimbrite	
Sample:	PMA 6	STA 24	PM 40	STA 25	PM 13	PM 34	STA 6B	STA 38	PMB 4 (fiamme)	PMC 116A (spatter)
Lat. (°S):	36·37672	36·38861	36·39402	36·30911	36·38033	36·39030	36·33336	36·46669	36·37527	36·35535
Long. (°W):	69·23782	69·29719	69·22036	69·29797	69·19828	69·21708	69·31183	69·29575	69·19707	69·33576
wt %										
SiO_2	67·61	67·83	67·24	66·45	60·08	54·43	58·39	52·75	65·16	63·93
TiO_2	0·423	0·385	0·447	0·399	1·270	1·705	1·312	1·874	0·620	0·645
Al_2O_3	15·58	15·26	15·63	15·59	17·41	17·53	18·04	17·63	17·34	17·56
$Fe_2O_3(T)$	3·02	2·94	2·95	2·89	5·69	8·44	6·12	8·9	3·38	3·53
MnO	0·125	0·124	0·108	0·120	0·131	0·141	0·140	0·154	0·089	0·098
MgO	0·31	0·28	0·32	0·29	1·40	3·41	1·81	3·38	0·61	0·58
CaO	0·70	0·64	0·71	0·70	3·19	6·47	4·15	6·86	1·95	1·98
Na_2O	5·61	5·55	6·13	5·46	5·81	4·66	5·34	4·52	5·66	5·76
K_2O	5·40	5·41	5·25	5·57	3·94	2·58	3·76	2·51	4·96	5·27
P_2O_5	0·09	0·06	0·08	0·08	0·41	0·49	0·56	0·66	0·17	0·18
LOI	0·43	0·43	0·32	1·39	0·31	<0·01	0·42	0·38	0·13	0·26
Total	99·29	98·92	99·18	98·94	99·63	99·83	100·04	99·62	100·10	99·81
ppm										
Sc	3	3	4	4	9	16	9	16	4	4
V	<5	<5	5	<5	51	154	77	171	15	17
Cr	<20	<20	<20	<20	<20	<20	<20	<20	<20	<20
Co	9	11	5	7	14	22	11	26	7	9
Ni	<20	<20	<20	<20	<20	30	<20	20	<20	<20
Cu	80	<10	20	<10	<10	20	<10	30	<10	<10
Zn	160	90	50	80	60	60	100	130	40	40
Ga	23	26	23	25	25	20	23	23	23	24
Rb	201	258	187	232	93	55	89	70	169	161
Sr	9	6	33	14	423	671	502	694	261	261
Y	45	48	40·5	43	25·6	23·6	45	30	26	28
Zr	897	829	851	846	479	307	479	341	565	576
Nb	95	109	78·9	99	53·6	33·1	53	40	73	73
Mo	13	19	5	15	<2	3	2	3	6	7
Sn	8	8	5	5	3	2	3	2	2	7
Sb	9·2	3·5	0·5	6	<0·2	<0·2	5·4	5·9	0·7	0·6
Cs	12·7	15·3	7·8	13·4	0·9	1·7	0·9	2	7·2	4·9
Ba	43	27	201	55	768	569	706	565	599	625
La	62·5	72·2	52·1	67·6	33·2	25·9	43·8	40·7	35·9	37·2
Ce	122	141	96	133	72·3	52·7	91·3	85·5	70·4	72·5
Pr	10·5	12·8	9·97	11·9	7·85	6·17	8·9	8·8	7·85	7·98
Nd	35·4	42·6	34·5	38·5	31·7	25·7	32·1	34·2	28·8	29
Sm	7·7	8·4	6·39	7·7	6·39	5·32	7·3	7·9	5·7	5·6
Eu	0·62	0·31	0·65	0·42	2·13	1·8	2·27	2·38	1·31	1·3
Gd	6·8	7·4	5·72	6·5	5·76	5·08	6·5	7·3	4·8	5
Tb	1·1	1·2	1·0	1·1	0·86	0·78	1·0	1·1	0·8	0·8
Dy	6·7	7·6	6·15	6·8	4·78	4·39	5·2	5·8	4·6	4·8
Ho	1·4	1·6	1·24	1·4	0·87	0·84	1·0	1·1	0·9	1
Er	4·8	5·3	4·04	4·7	2·52	2·38	3·0	3·2	2·9	3
Tm	0·8	0·89	0·71	0·77	0·38	0·343	0·44	0·47	0·47	0·48
Yb	5·4	6·1	4·75	5·3	2·51	2·13	2·8	2·9	3·4	3·5
Lu	0·86	0·93	0·71	0·83	0·38	0·313	0·43	0·42	0·57	0·62
Hf	20·5	20·5	18·5	19·9	10·8	6·8	10·6	8·1	12·8	13·2
Ta	8·2	9·5	6·52	8	4·23	2·9	4·0	3·1	5·2	5·3
W	132	136	72·5	79	73·9	98·8	43	73	91	112
Tl	2	1·9	0·11	0·3	0·18	0·19	0·4	0·1	0·1	0·2
Pb	25	21	12	12	11	8	13	9	14	16

(continued)

JOURNAL OF PETROLOGY | VOLUME 55 | NUMBER 1 | JANUARY 2014

Table 3: Continued

Unit:	Vitreous Trachytes (T pos)		Blocky Trachytes		Post-caldera Trachyandesites (T pos)				Portezuelo Ignimbrite	
Sample:	PMA 6	STA 24	PM 40	STA 25	PM 13	PM 34	STA 6B	STA 38	PMB 4 (fiamme)	PMC 116A (spatter)
Lat. (°S):	36·37672	36·38861	36·39402	36·30911	36·38033	36·39030	36·33336	36·46669	36·37527	36·35535
Long. (°W):	69·23782	69·29719	69·22036	69·29797	69·19828	69·21708	69·31183	69·29575	69·19707	69·33576
Th	34·3	42·1	29·1	37·3	15·8	8·89	15·3	10·3	25·4	25·8
U	9·2	11·9	7·64	10·1	3·03	2·23	3·2	2·9	7·6	7·4
Mg#	16·90	15·87	17·69	16·58	32·77	44·45	36·94	42·93	26·33	24·55
Normative										
Ol	–	–	–	–	–	–	–	0·07	–	–
Ne	–	–	–	–	–	–	–	–	–	–
Di	1·20	1·64	2·01	1·14	2·89	7·95	2·49	7·78	1·19	1·85
Hy	0·25	0·03	–	0·31	2·17	6·54	3·69	6·72	0·97	0·59
Qz	12·96	13·76	10·46	12·12	4·09	1·02	3·25	–	8·78	6·03

Unit:	Pre-caldera Trachytes				Post-caldera Basalts I and II			Pre-caldera Basalts		
Sample:	PM 15	PM 27	PY 10	PMA 76	PM 46	PY 14	PMC 104	PY 5	PY 15	STA 8
Lat. (°S):	36·38080	36·37394	36·41042	36·39885	36·33783	36·39061	36·37942	36·30256	36·38711	36·33461
Long. (°W)	69·18319	69·20119	69·11000	69·16695	69·39556	69·04269	69·30486	69·07819	69·04147	69·32453
wt %										
SiO$_2$	63·66	57·82	59·96	67·26	49·13	48·87	48·33	48·69	46·52	47·22
TiO$_2$	0·713	1·222	0·891	0·202	1·975	2·118	2·280	2·400	2·358	1·774
Al$_2$O$_3$	16·93	17·08	17·73	15·58	16·61	17·88	17·65	17·59	17·40	17·31
Fe$_2$O$_3$(T)	3·95	7·09	5·24	3·85	10·17	10·86	11·01	11·18	12·17	11·35
MnO	0·104	0·134	0·142	0·168	0·153	0·165	0·164	0·166	0·168	0·170
MgO	0·93	2·25	1·36	0·12	5·72	4·71	4·62	5·03	5·89	6·59
CaO	2·56	4·88	3·36	0·63	9·30	9·14	9·34	9·35	10·30	11·06
Na$_2$O	5·55	5·04	5·44	6·33	3·74	4·08	4·11	3·90	3·37	3·37
K$_2$O	4·21	3·03	3·73	4·92	1·56	1·74	1·44	1·72	0·94	1·06
P$_2$O$_5$	0·24	0·44	0·48	0·04	0·43	0·67	0·61	0·50	0·51	0·43
LOI	0·16	0·51	0·55	0·17	0·02	−0·27	−0·12	0·33	0·19	−0·08
Total	99·01	99·50	98·89	99·27	98·81	99·97	99·45	100·90	99·80	100·30
ppm										
Sc	4	8	6	4	26	20	23	22	25	29
V	30	89	39	<5	243	230	269	255	288	267
Cr	<20	<20	<20	<20	80	30	30	30	40	80
Co	8	16	9	5	29	29	42	34	31	44
Ni	<20	<20	<20	<20	50	<20	<20	20	<20	40
Cu	20	<10	20	<10	30	30	30	30	40	50
Zn	<30	60	110	160	60	130	80	130	150	120
Ga	17	20	19	26	20	20	23	21	19	21
Rb	116	83	77	214	26	26	20	27	14	21
Sr	361	599	487	5	640	857	769	751	757	679
Y	25·7	24·7	25	61	24·6	26	25	27	24	21
Zr	480	363	418	1081	175	209	188	197	131	132
Nb	44·1	37·4	48	101	19·5	27	27	27	16	14
Mo	5	4	<2	<2	<2	<2	<2	<2	<2	<2
Sn	1	2	2	7	1	2	2	2	3	1
Sb	<0·2	<0·2	9·2	6·9	<0·2	4·8	<0·5	6·5	8·4	<0·5
Cs	4·3	2·3	2·3	6·6	1	1	0·6	0·9	0·7	0·7
Ba	607	576	631	27	397	439	358	386	327	345
La	37·7	30·7	40·3	85·3	20	27·1	21·6	26·7	18·1	21·2
Ce	68·5	59·1	79·9	158	41·9	57·9	49·3	56·5	41·0	43·8
Pr	7·47	6·88	7·13	14·1	5·24	6·08	6·46	5·99	4·61	5·4

(continued)

Table 3: Continued

Unit:	Pre-caldera Trachytes				Post-caldera Basalts I and II			Pre-caldera Basalts		
Sample:	PM 15	PM 27	PY 10	PMA 76	PM 46	PY 14	PMC 104	PY 5	PY 15	STA 8
Lat. (°S)	36·38080	36·37394	36·41042	36·39885	36·33783	36·39061	36·37942	36·30256	36·38711	36·33461
Long. (°W)	69·18319	69·20119	69·11000	69·16695	69·39556	69·04269	69·30486	69·07819	69·04147	69·32453
Nd	27·2	27	27	49·8	23·3	26·2	29·5	24·4	21·7	23
Sm	5·04	5·24	5·9	10·1	5·23	6·9	6·7	6·3	6·0	5·6
Eu	1·28	1·74	1·76	0·42	1·84	2·22	2·2	2·17	2·13	1·88
Gd	4·42	5	5·2	9	5·19	6·5	6·8	6·1	6·2	5·2
Tb	0·73	0·81	0·8	1·5	0·85	0·9	1	0·9	0·9	0·8
Dy	4·34	4·35	4·4	8·8	4·57	4·8	5·4	4·9	4·6	4·2
Ho	0·84	0·84	0·9	1·9	0·86	0·9	1	0·9	0·9	0·8
Er	2·61	2·49	2·6	5·9	2·35	2·8	2·7	2·7	2·6	2·2
Tm	0·43	0·39	0·42	0·96	0·32	0·41	0·38	0·37	0·37	0·31
Yb	2·9	2·54	2·9	6·6	1·99	2·6	2·4	2·2	2·4	1·9
Lu	0·451	0·36	0·44	1·03	0·29	0·36	0·39	0·30	0·36	0·29
Hf	10·6	8·3	9·7	22·8	4·3	5·4	4·7	4·8	4·1	3·3
Ta	4·39	3·51	4·4	8·3	1·78	2·5	2·3	2·1	1·4	1·3
W	63·6	89·3	55	68	85·6	91	158	70	49	50
Tl	0·07	0·18	0·7	0·6	0·09	0·5	<0·1	0·3	0·4	<0·1
Pb	5	10	16	25	5	<5	<5	<5	<5	300
Th	19·5	13·7	16	32·8	3·2	3·2	2·4	3·3	2·2	3·3
U	5·87	4·01	2·9	8·6	0·94	1	0·7	1·0	0·7	0·9
Mg#	31·80	38·60	33·95	5·81	52·70	46·21	45·39	48·94	47·12	53·49
Normative										
Ol	–	–	–	–	7·88	6·91	6·34	9·61	6·89	10·49
Ne	–	–	–	–	0·60	2·52	2·41	1·36	2·15	2·23
Di	1·98	5·30	0·72	2·22	15·99	12·90	13·92	15·03	13·96	20·02
Hy	1·58	4·52	3·82	–	–	–	–	–	–	–
Qz	9·52	5·06	5·96	10·58	–	–	–	–	–	–

Magnesium number calculated as the molar proportion of $100MgO/(MgO + FeO_{total})$. Normative minerals are expressed as wt %.
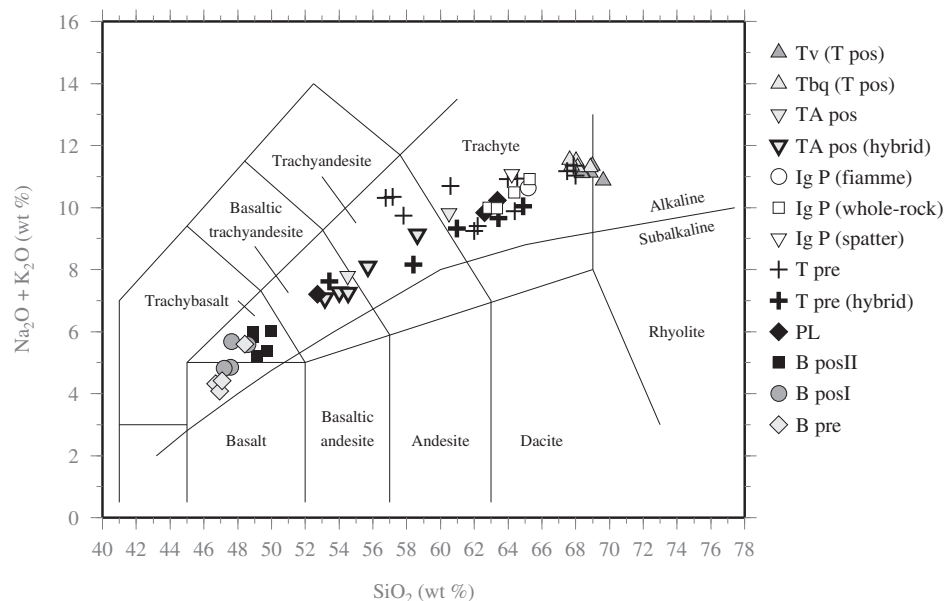
Fig. 5. Total alkalis vs silica (TAS) classification diagram for the PMVF volcanic rocks. Line separating the subalkaline from the alkaline field is after Irvine & Baragar (1971). Abbreviations as in Fig. 2.

alkalis). The small number of Payún Liso analyses suggest a similar trend to that of Payún Matrú (Fig. 5).

The total alkalis–silica (TAS) diagram (Fig. 5) shows two gaps in the silica content of the PMVF rocks. One gap divides the lavas of the basaltic fields from those of the polygenetic volcanoes, with a hiatus in silica content of near 3 wt %. The other gap, around 66 wt % SiO_2, divides the trachytic field into trachytes with less than 65·3 wt % SiO_2 and trachytes with more than 67·5 wt % SiO_2.

Trachytic rocks of the polygenetic volcanoes are mostly silica-saturated (with neither quartz nor nepheline in the norm) to silica-oversaturated to variable degrees (normative quartz up to about 15 wt %). Only a few intermediate lavas of the pre-caldera stage are slightly undersaturated (Ne < 2 wt %). Rocks of the PMVF are metaluminous, and only a few trachytes are weakly peralkaline [with molar $(Na_2O + K_2O)/Al_2O_3 < 1·05$]. The weakly peralkaline rocks correspond to the most silicic trachytes that form two post-caldera lavas and one pre-caldera lava. According to their Al_2O_3 and FeO_T abundances, these peralkaline lavas are defined as comenditic trachytes (Macdonald, 1974).

There is a general tendency towards an increase in SiO_2 and a lesser degree of silica-undersaturation in the latest Post-caldera Basalts II, in comparison with the Pre-caldera Basalts, although there is some overlap between these units (Fig. 5 and Table 3). The Post-caldera Basalts I have silica contents and amounts of normative nepheline that overlap and are intermediate between those of the younger and older basaltic units. Basalts belonging to the post-caldera stage are better represented in the western basaltic field, whereas Pre-caldera Basalts are more abundant in the eastern basaltic field, owing to the abundance of post-caldera lavas in the western basaltic field that cover most of the oldest lavas (Hernando et al., 2012).

Harker variation diagrams for major and minor elements are shown in Fig. 6. The Al_2O_3 content is relatively constant in rocks with less than 66 wt % SiO_2, but is lower in the most silicic rocks. The PMVF rocks show a negative correlation between $Fe_2O_3(T)$, MgO and CaO vs SiO_2. MgO (0·12–7·3 wt %) shows a greater dispersion in the basaltic fields than Fe_2O_3 (T) (2·9–12·4 wt %) and CaO (0·6–11·1 wt %). Na_2O (3·2–6·3 wt %) and K_2O (0·9–5·6 wt %) contents positively correlate with SiO_2. The TiO_2 contents are high (1·77–2·36 wt % in the basaltic units) and decrease with increasing silica content. P_2O_5 shows variable abundances in Pre- and Post-caldera Basalts, whereas in the Payún Matrú and Payún Liso rocks it decreases linearly with SiO_2 content. The values of the Mg# [molar proportion of $100MgO/(MgO + FeO_{total})$] for the Pre- and Post-caldera Basalts vary between 45 and 55, and decrease linearly with silica content (not shown in Fig. 6).

Trace elements

Representative trace element compositions are listed in Table 3. Variation diagrams versus SiO_2 for some trace elements are shown in Fig. 7. Ba contents are relatively low in the basic lavas of the basaltic fields, and are higher in the intermediate rocks of Payún Matrú and Payún Liso, with an inflection around 66 wt % SiO_2, decreasing strongly in the most silicic trachytes. Sr has a negative correlation, with greater dispersion in the basic compositions. Zr, Nb and Rb show similar trends with positive slopes and with greater dispersion in the silicic samples. The Cr and Ni contents are variable in the basaltic units (30–180 ppm and < 20–90 ppm, respectively), and in most of the Payún Matrú lavas are below the detection limit of 20 ppm. Incompatible element versus incompatible element plots (not shown) show a good positive correlation; for example, Ta vs Nb ($r^2 = 0·93$), Th vs Rb ($r^2 = 0·96$), Zr vs Hf ($r^2 = 0·98$) and Zr vs Nb ($r^2 = 0·87$).

REE were normalized to chondritic abundances using the normalization constants of Sun & McDonough (1989) (Fig. 8). The pre- and post-caldera basaltic lavas show an enrichment of the light REE (LREE) with respect to the heavy REE (HREE), which is typical for ocean island basalt (OIB; e.g. Sun & McDonough, 1989). These lavas are also characterized by a flattening of the REE pattern from Dy to Lu in comparison with the LREE and middle REE (MREE), with a ratio of $(Dy/Lu)_N$ between 1·27 and 1·63. Pleistocene–Holocene arc basaltic lavas from the Planchón, San Pedro, Cerro Azul, Antuco and Llaima volcanoes, located at similar latitudes to the PMVF, are plotted in Fig. 8 for comparison (Tormey et al., 1991); these have lower $(La/Yb)_N$ and lower total REE contents. In the Payún Matrú rocks the negative slope in REE patterns persists, with an increase in the REE content (except for Eu) and a flattening in the HREE [with ratios of $(La/Sm)_N$ between 6·5 and 2·7, and $(Gd/Yb)_N$ between 0·9 and 2]. The $(La/Yb)_N$ ratios of the whole volcanic field are mostly in the range of 5–10, although a few lavas from Payún Matrú and Payún Liso have higher ratios (Fig. 9a). The basaltic and trachybasaltic lavas do not have a significant Eu anomaly, and the Eu/Eu* ratio is generally slightly higher than unity (Fig. 9b), suggesting that plagioclase is not a major phase involved in fractional crystallization processes. In contrast, the Post-caldera Trachytes lithofacies and the most silicic Pre-caldera Trachytes have a marked negative Eu anomaly, with Eu/Eu* between 0·12 and 0·42. The remaining Pre-caldera Trachytes do not have a significant Eu anomaly or it is slightly negative. The Portezuelo Ignimbrite samples have both positive and negative Eu anomalies (Fig. 9b). The former are present in whole-rock analyses (samples PM 24, PM 26 and PM 43, with Eu/Eu* between 1·32 and 1·59) and the latter are present in fiamme, spatter clasts and one whole-rock analysis (sample PM 14). The REE abundances of
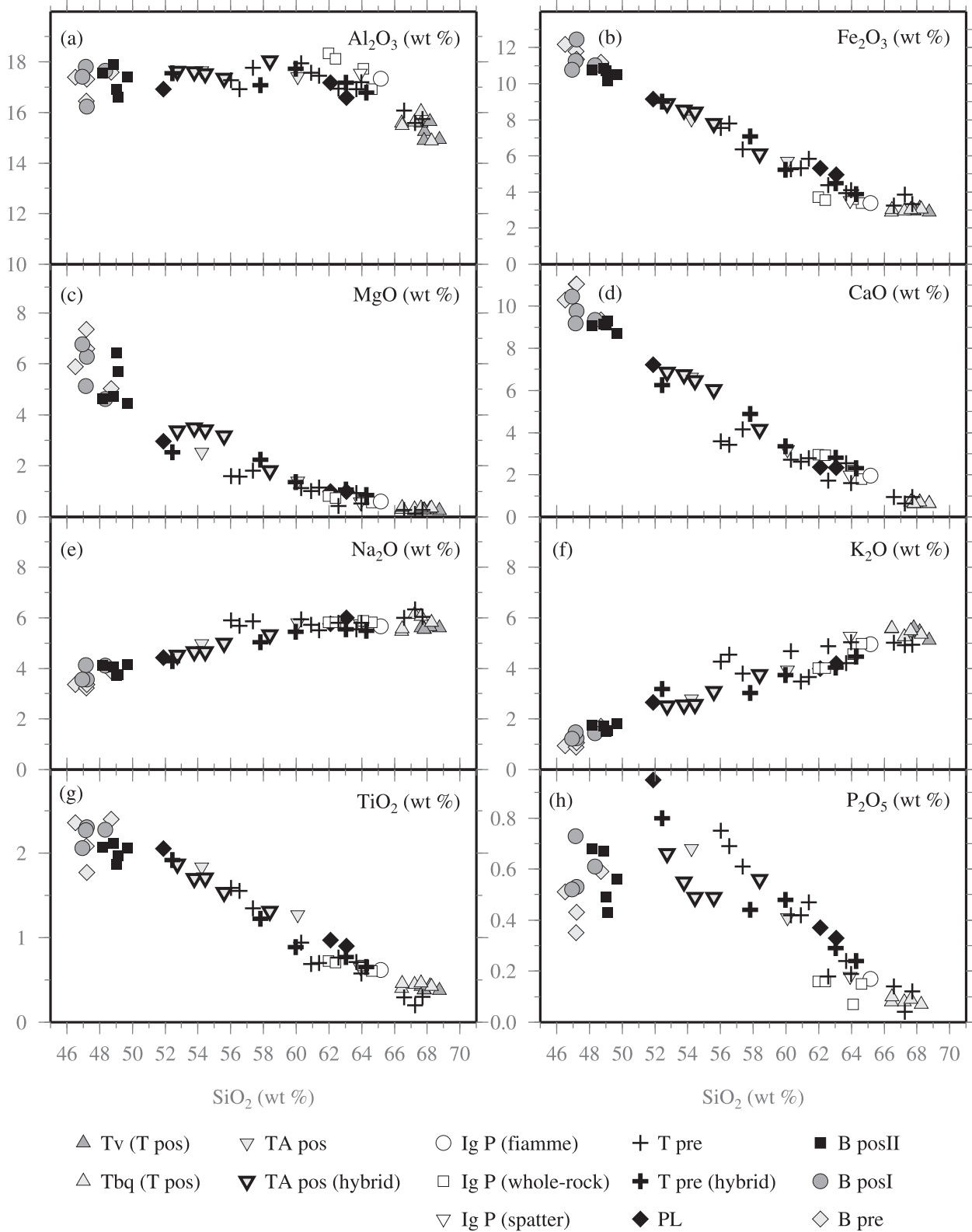
Fig. 6. Harker variation diagrams for major and minor elements in the PMVF rocks. Abbreviations as in Fig. 2.
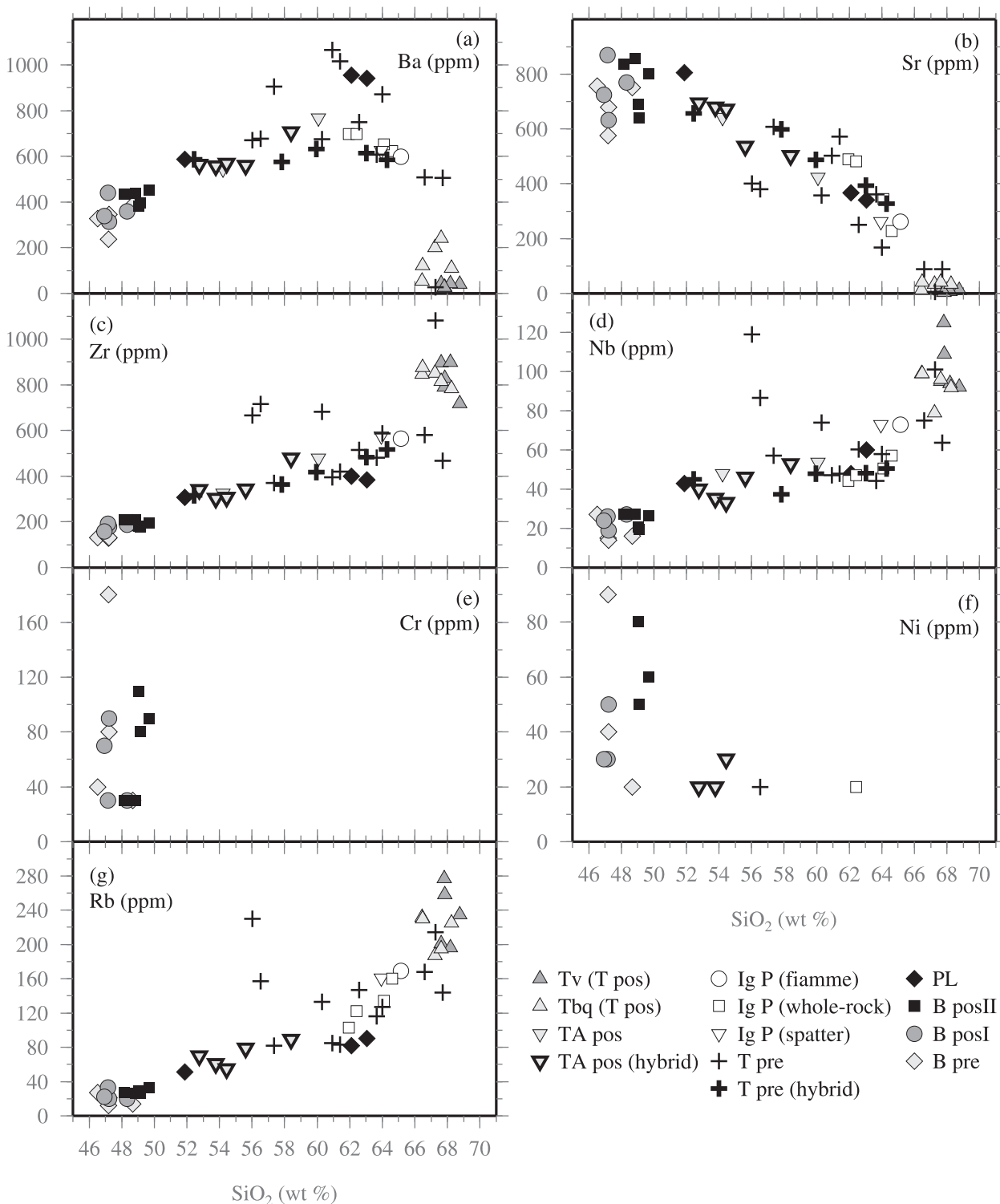
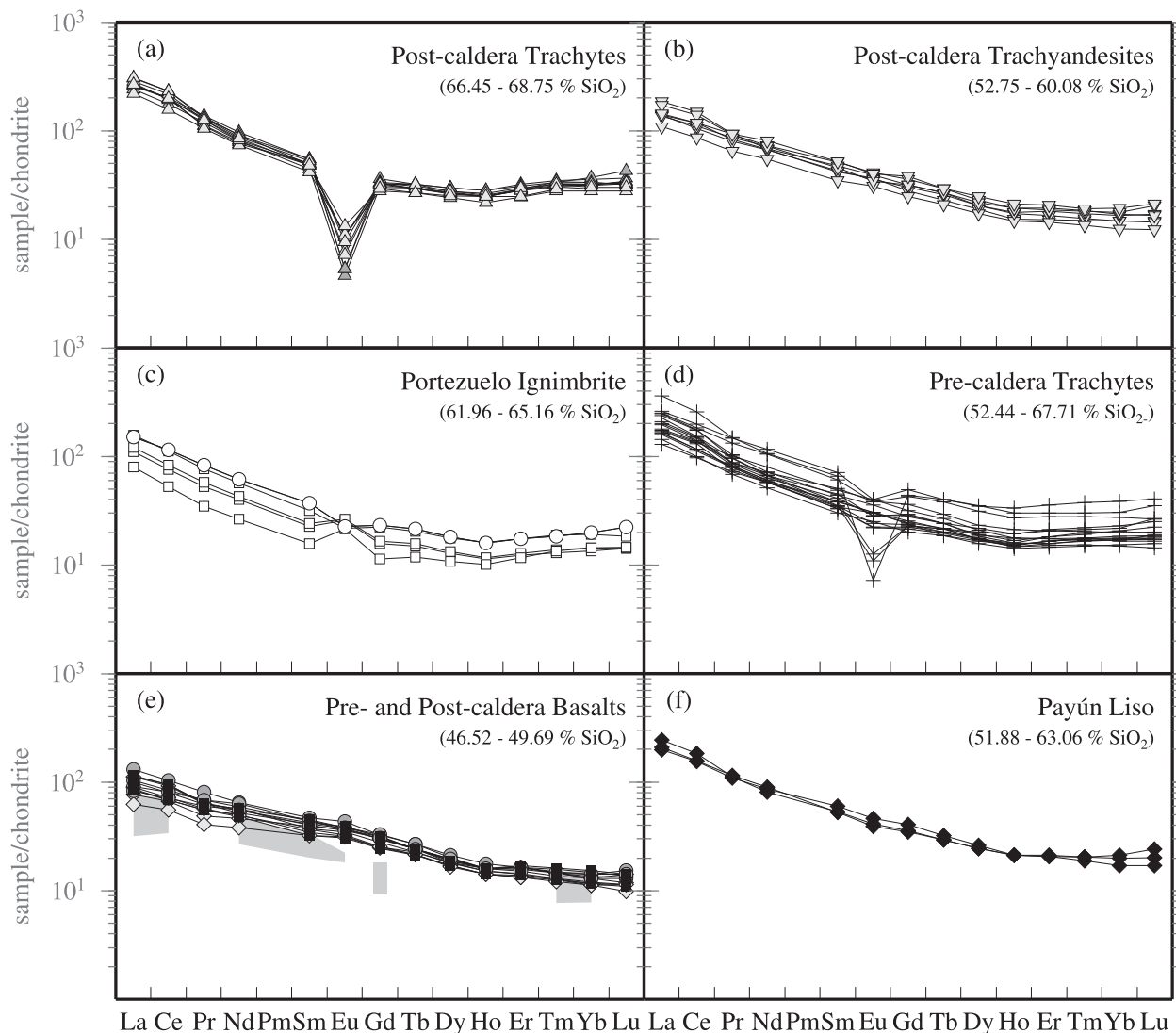**Fig. 7.** Selected trace elements vs SiO_2 (wt %) for rocks of the PMVF. Abbreviations as in Fig. 2.

Fig. 8. Chondrite-normalized REE diagrams for the volcanic units of the PMVF. Symbols as in Fig. 2. Gray shaded field in (e) represents the Pleistocene–Holocene arc basalts (Tormey *et al.*, 1991).

whole-rock samples PM 24, PM 26 and PM 43 of the Portezuelo Ignimbrite are lower than those of the other samples of the ignimbrite. Because the former are the samples with significant vapour-phase crystallization, they are not considered in the following discussion, and the fiamme, spatter clasts and PM 14 samples are considered to be the most representative of the composition of the Portezuelo Ignimbrite.

The presence of both positive and negative Eu anomalies in whole-rock analyses of the Portezuelo Ignimbrite may be due to lithic clast contamination, although the lithic clasts in the ignimbrite are all volcanic and mostly trachytic and trachyandesitic and there are no trachytes in the PMVF with such a positive Eu anomaly and, thus,

this explanation seems unlikely. An alternative explanation is that in some samples there is an excess of feldspars in the matrix relative to fiamme (e.g. by depletion of fine ash). The percentage of crystals in the matrix (up to around 20%) is generally higher than in the fiamme and pumice clasts (generally less than 10%), and the percentage of plagioclase is slightly higher in those samples with a positive Eu anomaly (15–20%) than in the whole-rock sample with the negative Eu anomaly (~10%). The positive Eu anomaly in three of the four whole-rock analyses could be linked to an excess of plagioclase in the matrix, although there are trachytes with similar feldspar abundances without a positive Eu anomaly.
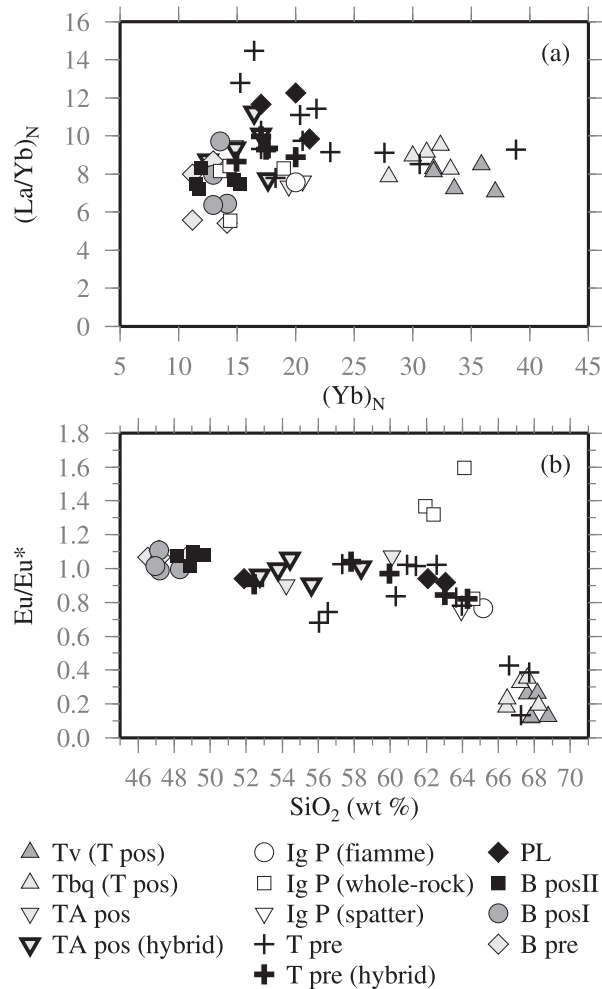
Fig. 9. (a) $(Yb)_N$ vs $(La/Yb)_N$. Elements normalized to chondritic meteorites according to Sun & McDonough (1989). (b) Eu anomalies for the units of the PMVF. Symbols as in Fig. 2.

Incompatible elements were normalized to mid-ocean ridge basalt (MORB) according to Pearce (1983) (Fig. 10). Lavas of the basaltic units show an enrichment of the most incompatible elements, which is typical for intraplate alkali basalts (Pearce, 1982). They do not have the Nb–Ta negative anomaly that characterizes subduction zones (e.g. Pearce, 1982; Baier *et al.*, 2007), and that is present in the contemporaneous arc basalts at similar latitudes (grey field in Fig. 10e) (Tormey *et al.*, 1991). The arc basalts also show generally lower contents of incompatible elements compared with the back-arc PMVF basalts (Fig. 10e). The tendency in the MORB-normalized patterns from basalts to the most silicic trachytes is one of increasing content of incompatible elements and, with the exception of a few negative troughs in certain elements, the overall shape of the patterns remains the same (Fig. 10). Negative troughs are present in Sr, Ba, P_2O_5 and TiO_2; these are prominent

in the Post-caldera Trachytes and the most silicic Pre-caldera Trachytes, and less marked in the Portezuelo Ignimbrite and most of the Pre-caldera Trachytes. In the Post-caldera Trachyandesites and a few Pre-caldera Trachytes, the troughs are small or absent. The compositions of the Payún Liso lavas show similar trends to those of some Payún Matrú lavas (Fig. 10f). The negative troughs in Sr, Ba, P_2O_5 and TiO_2 suggest the fractionation of minerals such as feldspars, Fe–Ti oxides and apatite in the trachytes (especially the most silicic ones), as also suggested by the decrease in these elements with increasing silica (Figs 6 and 7).

Sr and Nd isotopes

Whole-rock $^{87}Sr/^{86}Sr$ and $^{143}Nd/^{144}Nd$ ratios determined for rocks from the basaltic fields and Payún Matrú are presented in Table 4 and Fig. 11. In the PMVF, Nd isotopic compositions are relatively constant from basaltic to trachytic lavas, ranging from 0·512743 to 0·512834, whereas $^{87}Sr/^{86}Sr$ varies between 0·703813 and 0·704841 (Fig. 11a). The basaltic field lavas and most of the Payún Matrú rocks show a more limited range in their $^{87}Sr/^{86}Sr$ ratio, from 0·703813 to 0·704132, whereas the majority of the most silicic and latest lavas of the Post-caldera Trachytes unit have a significantly higher $^{87}Sr/^{86}Sr$ (Fig. 11b). The Sr contents of these post-caldera lavas are low, between 6 and 41 ppm, in clear contrast to the other Payún Matrú samples analyzed for their Sr isotopic ratios, which have Sr abundances between 327 and 694 ppm. The significantly higher $^{87}Sr/^{86}Sr$ ratio in these Post-caldera Trachyes may be a consequence of their low Sr contents, which makes them susceptible to contamination (pre- or post-eruptive). The isotopic compositions of the basaltic and trachybasaltic samples are typical for continental sodic alkali basalts (Farmer, 2003). The Sr and Nd isotopic compositions of lavas from the basaltic fields and Payún Matrú indicate a moderately depleted mantle source relative to the Bulk Silicate Earth (BSE), plotting within the mantle array between the PREMA–HIMU and BSE reservoirs (Fig. 11a; Zindler & Hart, 1986).

MANTLE SOURCE

The isotopic and trace elements characteristics of the PMVF basalts suggest an asthenospheric source, without significant lithospheric interaction. According to Nd–Sr isotopic data for continental lithosphere-derived mantle xenoliths from around the world, the isotopic composition of the continental lithospheric mantle commonly has a lower εNd (<0) and higher $^{87}Sr/^{86}Sr$ (>0·7045) compared with the sublithospheric mantle (Farmer, 2003), but this may vary depending on the mantle region considered. A comparison between the Sr–Nd isotopic compositions of the PMVF basalts and those of mantle xenoliths from the region is not possible, as the scarce xenoliths found in
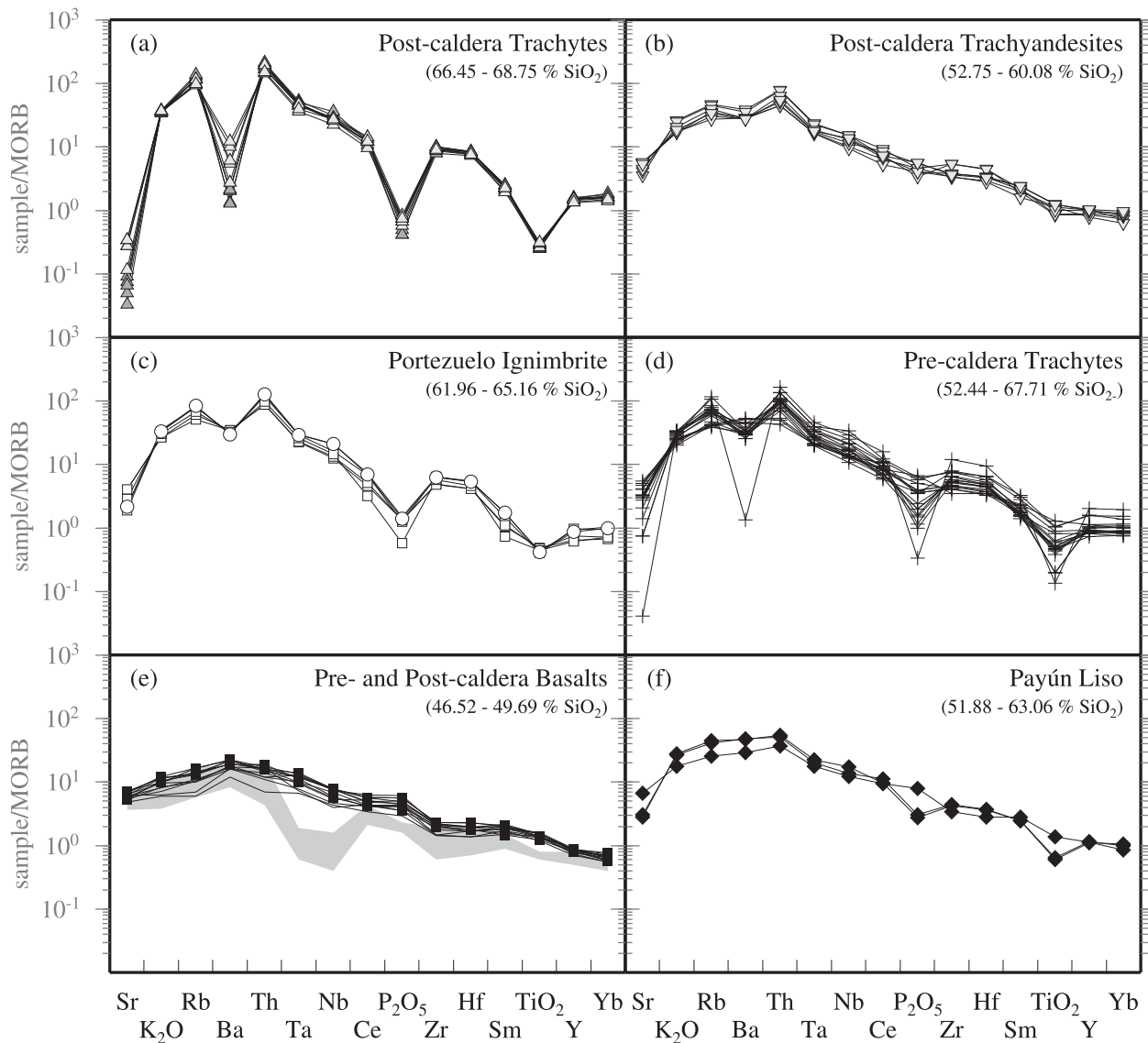
Fig. 10. MORB-normalized incompatible trace element patterns for the PMVF rocks, after (Pearce, 1983). Symbol keys and abbreviations as in Fig. 5. Gray shaded field in (e) represents the Pleistocene–Holocene arc basalts (Tormey *et al.*, 1991).

Payenia have not been analysed for their Sr and Nd isotope composition and, also, it is unclear whether they are derived from the lithospheric or sublithospheric mantle (Bertotto *et al.*, 2009, and references therein). The PMVF basalts have a geochemical similarity to OIB, which typically represent magmas generated in the asthenosphere (Fitton *et al.*, 1991; Farmer, 2003). However, OIB may also be generated by melting of metasomatized lithospheric mantle (Niu & O'Hara, 2003; Pilet *et al.*, 2005, 2008, 2011).

In a variation diagram of La/Nb vs La/Ba the basaltic units of the PMVF plot within the OIB field (Fig. 12), and differ from those located along the arc axis. Differences

such as the relatively high Nb and low Ba contents of the PMVF basalts with respect to the arc basalts (Fig. 12), and the lack of Nb–Ta negative anomalies, indicate a different petrogenesis for the back-arc basalts from those present in the volcanic arc. No subduction fluid influence seems to be present in the back-arc basalts of the PMVF, which are separated by 150 km from the axis of the contemporaneous volcanic arc. The Sr and Nd isotopic compositions of the PMVF basalts are similar to those of Auca Mahuida, Tromen and the Rio Colorado region (Fig. 1), with a proposed asthenospheric mantle source (Kay *et al.*, 2004, 2006*a*); they are also similar to the contemporaneous arc basalts at similar latitudes in Payenia, which have a

Table 4: Sr–Nd isotopic compositions of PMVF rocks

Unit	Sample	Lat. (°S)	Long. (°W)	$^{87}Sr/^{86}Sr$	± ppm	± abs	$^{143}Nd/^{144}Nd$	± ppm	± abs
Tv (T pos)	PMA 6	36·37672	69·23782	0·704768	12	0·000008	0·512757	15	0·000008
	STA 24	36·38861	69·29719	0·704666	10	0·000007	0·512770	14	0·000007
Tbq (T pos)	PM 40	36·39403	69·22036	0·704123	6	0·000004	0·512743	10	0·000005
	STA 25	36·30911	69·29797	0·704841	11	0·000008	0·512767	12	0·000006
TA pos	PM 13	36·38033	69·19828	0·704029	7	0·000005	0·512767	10	0·000005
	PM 34	36·3903	69·21708	0·704082	5	0·000004	0·512766	14	0·000007
	STA 6B	36·33336	69·31183	0·704082	7	0·000005	0·512773	13	0·000007
	STA 38	36·46667	69·29575	0·704132	7	0·000005	0·512761	17	0·000009
T pre	PM 15	36·37625	69·19828	0·704079	6	0·000004	0·512769	12	0·000006
	PM 27	36·3808	69·18319	0·704087	8	0·000006	0·512761	14	0·000007
	PY 10	36·41042	69·11000	0·703855	7	0·000005	0·512807	15	0·000008
B posII	PM 46	36·33783	69·39556	0·703924	7	0·000005	0·512746	13	0·000007
B pre	PY 5	36·30256	69·07819	0·703813	9	0·000006	0·512834	11	0·000006
	PY 15	36·38711	69·04147	0·703853	11	0·000008	0·512792	15	0·000008
	STA 8	36·33461	69·32452	0·703925	8	0·000006	0·512787	12	0·000006

Tv, Vitreous Trachytes lithofacies; Tbq, Blocky Trachytes lithofacies; T pos, Post-caldera Trachytes; TA pos, Post-caldera Trachyandesites; T pre, Pre-caldera Trachytes; B posII, Post-caldera Basalts II; B pre, Pre-caldera Basalts.

proposed mixed source, with both lithospheric and asthenospheric components (Tormey *et al.*, 1991).

The chemical similarity of the PMVF basalts to OIB is a feature that is repeated in other continental volcanic fields located in intraplate or back-arc settings, such as the Rio Grande Rift in the western USA (e.g. Leat *et al.*, 1990; Gibson *et al.*, 1992) and New Zealand (e.g. Timm *et al.*, 2010). Incompatible trace element ratios normalized to primitive mantle (Sun & McDonough, 1989) of the Pre- and Post-caldera Basalts, such as Rb/Sr (0·6–1·4), U/Pb (0·9–4·4), Ba/Nb (1·3–2·5), Ce/Pb (0·7–3) and Nb/U (0·5–1·1), span those of alkaline OIB and alkaline continental basalts (Pilet *et al.*, 2011), but they do not share the positive Nb anomaly with respect to U and La (i.e. Nb/U >1 and Nb/La >1) common in those alkaline lavas (with the exception of only one post-caldera sample).

With regard to a possible metasomatized lithospheric mantle source, Pilet *et al.* (2011) proposed that the source of alkaline magmas may be related to lithospheric metasomatism, and found that amphibole-bearing veins in the lithosphere may be significant components in the sources of alkaline OIB and continental basalts. Metasomatized lithospheric mantle does not seem to make a major contribution in the petrogenesis of PMVF magmas, because their trace element ratios and concentrations are significantly different from those of melts derived from hydrous veins within metasomatized lithospheric mantle (as modelled by Pilet *et al.*, 2011). Among these differences are the

following: (1) the absence of a marked positive Nb anomaly in the PMVF basalts with respect to U and LREE (with the exception of only one sample), which is present in the model owing to the compatibility of Nb in amphibole; (2) the relatively high ratio of Ba/Nb and the generally lower ratios of U/Pb, Ce/Pb and Nb/U (normalized to primitive mantle) in the PMVF basalts with respect to the proposed model melts; (3) higher ratios of primitive mantle normalized Sr/REE in the PMVF basalts; (4) negative Pb anomalies in primitive mantle normalized trace element patterns in the metasomatized lihospheric mantle model whereas Pb has variable behavior in the PMVF basalts, with some samples with a positive Pb anomaly and others with a negative Pb anomaly; (5) higher HREE contents and lower $(La/Yb)_N$ in the PMVF basalts with respect to the model melts, which could be related to the use of a garnet-bearing asthenospheric source for the metasomatizing fluids in the Pilet *et al.* (2011) model. The positive anomalies in Pb and Sr (and also Zr and Hf) with respect to LREE in some samples could be due to the fractionation of accessory phases such as apatite, which incorporate REE but not Pb and Sr (Pilet *et al.*, 2011).

The nature of the mantle source of the PMVF basalts could be constrained by the study of mantle xenoliths brought to the surface by the basaltic lavas. Unfortunately, no xenoliths have been found thus far in lavas and scoria cones in the study area, although further to the SE basalt-hosted xenoliths have been found in three
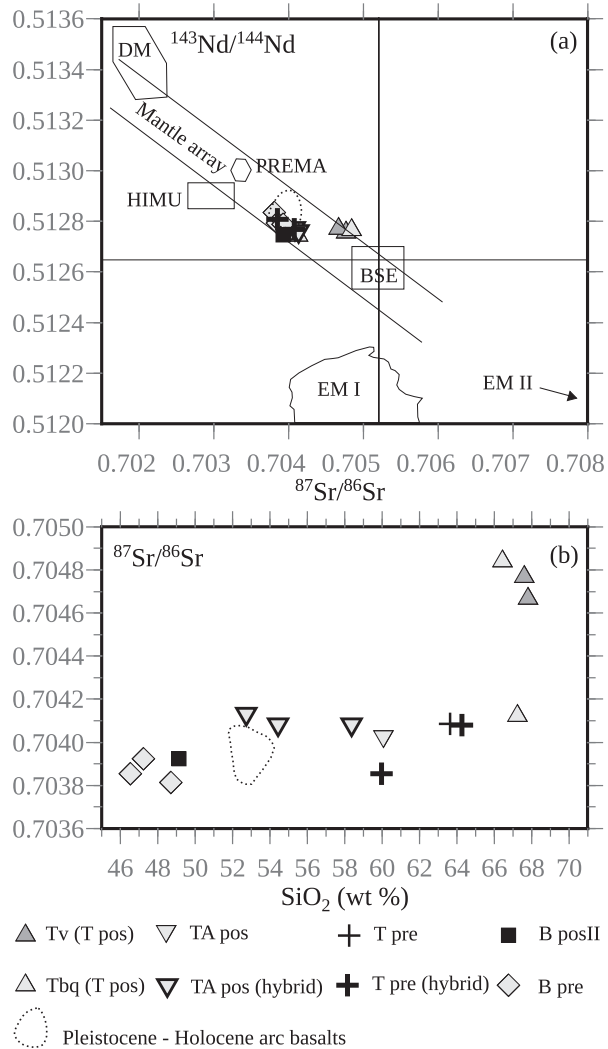
Fig. 11. (a) $^{87}Sr/^{86}Sr$ vs $^{143}Nd/^{144}Nd$ diagram, showing the mantle reservoirs as defined by Zindler & Hart (1986). Rocks of the PMVF lie within the mantle array, and are slightly depleted relative to BSE. (b) Variation of $^{87}Sr/^{86}Sr$ with silica content. Most of the Post-caldera Trachytes samples have higher $^{87}Sr/^{86}Sr$. Data for Pleistocene–Holocene basaltic and basaltic andesitic arc lavas are from Tormey *et al.* (1991).

Fig. 12. La/Nb vs La/Ba for basalts and trachybasalts of the PMVF (after Fitton *et al.*, 1991), and basalts of the Pleistocene–Holocene volcanic arc (field with dotted outline) (Tormey *et al.*, 1991). The OIB field is based on more than 900 analyses of OIB from various ocean islands (Fitton *et al.*, 1991).

localities (Bertotto *et al.*, 2009, and references therein). These xenoliths are spinel peridotites, with a minimum depth of formation of 45–70 km (Bertotto *et al.*, 2009). Based on the whole-rock geochemistry of the host basalts, particularly the REE slope and $(Ti/Y)_N$ values >1, Bertotto *et al.* proposed that they originated from a garnet peridotite mantle source. With the exception of only one sample with relatively high $(La/Yb)_N$, the REE slopes of the basalts located east of the PMVF are similar to those of the PMVF basalts.

The moderately elevated $(La/Yb)_N$ ratios (<10), the nearly flat slope in HREE [$(Dy/Lu)_N$ between 1·27 and 1·63] and the high chondrite-normalized Lu contents (between 9·8 and 15·3) in the PMVF basaltic lavas suggest that garnet did not exert a major control on REE contents. The PMVF basalts have MORB-normalized Ti/Y ratios ranging from 1·54 to 2·00. Given that the $(Ti/Y)_N$ ratio for MORB varies from ~0·60 to 1·34, and that for OIB varies from ~1·34 to 3·36 (Pearce, 1982), then the $(Ti/Y)_N$ ratios of the PMVF basalts lie within the low $(Ti/Y)_N$ OIB range, which may not have a garnet-bearing source. Therefore, the $(Ti/Y)_N$ ratio of PMVF basalts is not considered diagnostic of garnet in the source, although a small contribution of garnet to the PMVF basalts cannot be dismissed.

The REE contents may indicate that the mantle source of the PMVF primary magmas was a spinel lherzolite or, alternatively, that garnet in the source was completely melted and thus the depletion in HREE is not observed; this would require a relatively high degree of partial melting depending on the garnet content of the lherzolite. Kay (2002) modelled the basalts of Payenia by derivation from an enriched mantle source by 2–8% partial melting, and thus total fusion of garnet in the source would seem unlikely. Therefore, the mantle source of magmas is probably a spinel peridotite (spinel stability field between 30 and 80 km).
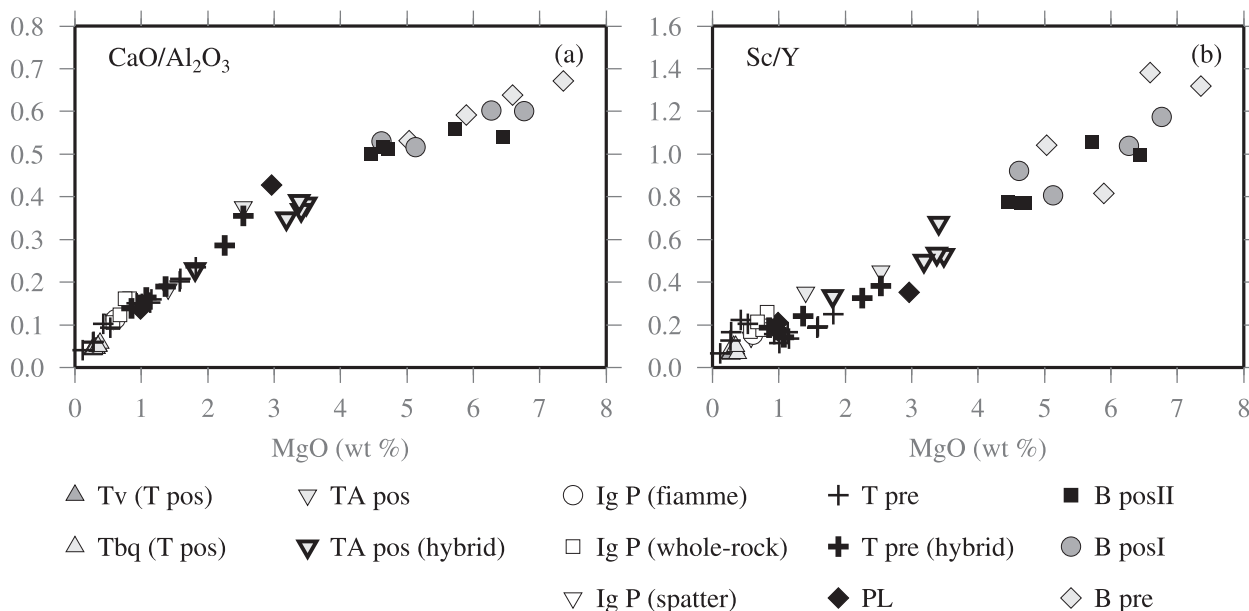
Fig. 13. Covariations of CaO/Al$_2$O$_3$ and Sc/Y vs MgO in the PMVF rocks. Symbols as in Fig. 2.

MAGMA EVOLUTION

The Mg# and Ni and Cr contents of the PMVF basalts indicate their non-primary nature, as is the case for other (but not all) basaltic lavas of Payenia (Bermúdez & Delpino, 1989). Their REE and incompatible elements patterns do not show negative Eu or Sr anomalies, which suggests that plagioclase is not a significant fractionated phase (Pearce, 1982), although it is generally present as a phenocryst. The marked decrease in elements such as Cr and Ni with increasing SiO$_2$ (Fig. 7e and f) suggests that fractionation of olivine and clinopyroxene played a key role in the early stage of the evolution of the suite. The covariations of MgO vs CaO/Al$_2$O$_3$ and MgO vs Sc/Y, with positive correlations in both diagrams (Fig. 13), confirm that clinopyroxene has been fractionated (Mattsson & Oskarsson, 2005). Fe–Ti oxides may also have been fractionated, owing to the variations in Ti and Fe observed.

The isotopic composition indicates an absence or non-significant upper crustal contamination in the basaltic and trachybasaltic lavas, although they may have been contaminated by lower crustal basic rocks with similar isotopic ratios. In the pre-caldera and early post-caldera rocks of Payún Matrú, the ^{87}Sr/^{86}Sr data also suggest insignificant crustal contamination (Fig. 11b). Most Post-caldera Trachytes lavas show a correlation between SiO$_2$ and ^{87}Sr/^{86}Sr (Fig. 11b) and an increase in ^{87}Sr/^{86}Sr with time, which suggests a moderate role for crustal contamination in the latest lavas of the volcano.

The basement of the volcanic field partly comprises sediments of the Neuquén Basin; the moderate contamination in the Post-caldera Trachytes may be due to assimilation of limestones and evaporites from this basin. Limestones of the Jurassic Calabozos Formation of the northern Neuquén Basin have ^{87}Sr/^{86}Sr between 0·706943 and 0·707083 and Sr contents between 252 and 549 ppm (Valencio *et al.*, 2003; Cagnoni *et al.*, 2006), and Jurassic marine evaporites from the Tábanos and Auquilco Formations have ^{87}Sr/^{86}Sr between 0·706793 and 0·706839 (Lo Forte *et al.*, 2005). There is no simple correlation between age and degree of crustal contamination within the Post-caldera Trachytes. Of the four lava flows of this unit for which the Sr isotopic composition has been analyzed, two of them are dated at 7 ka (Blocky Trachytes lithofacies, Germa *et al.*, 2010) and 20 ka (Vitreous Trachytes lithofacies), and the younger lava is the one that does not show significant contamination.

Assimilation–fractional crystallization (AFC) modelling was performed following the equations presented by DePaolo (1981) to explain the Sr contents and ^{87}Sr/^{86}Sr of the Post-caldera Trachytes (Fig. 14). The starting composition was a silica-poor trachyte (sample PM 13, without textural evidence of hybridization) with 423 ppm of Sr and ^{87}Sr/^{86}Sr of 0·704029. The contaminant chosen for the calculations is a limestone of the Calabozos Formation with 408 ppm of Sr and ^{87}Sr/^{86}Sr of 0·707011 (Valencio *et al.*, 2003). Only Sr and ^{87}Sr/^{86}Sr values were used in the calculations, because of the lack of ^{143}Nd/^{144}Nd and other trace element information for the Calabozos Formation limestones. Low mass assimilation to mass crystallization rates (*r*) can produce the relatively high ^{87}Sr/^{86}Sr and low Sr contents observed in the majority of the Post-caldera Trachytes (Fig. 14).
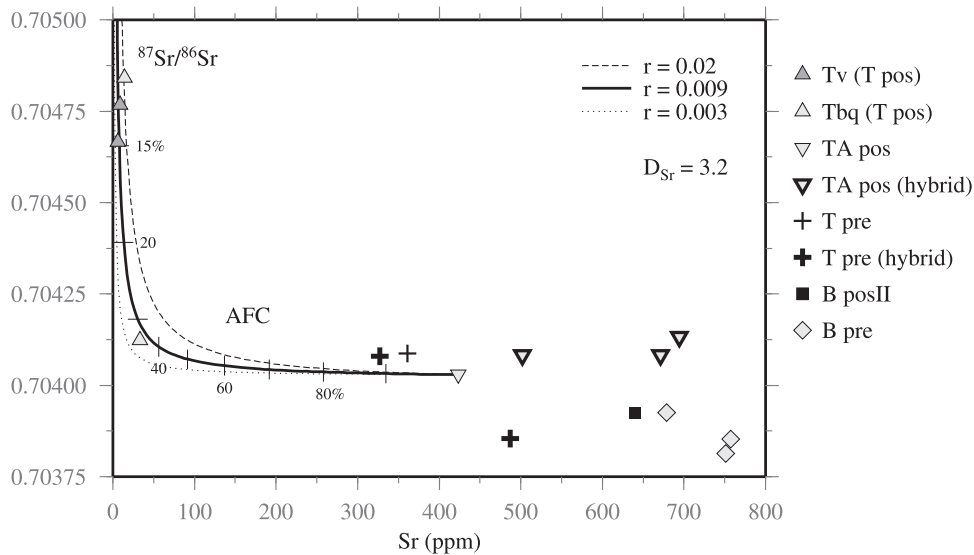
Fig. 14. Variation of $^{87}Sr/^{86}Sr$ vs Sr (ppm) showing AFC models (DePaolo, 1981) for the PMVF evolved rocks, with sample PM 13 (silica-poor trachyte of the Post-caldera Trachyandesites unit) as the starting composition for the AFC curves, and a limestone from the Calabozos Formation (Jurassic) with 408 ppm Sr and an $^{87}Sr/^{86}Sr$ ratio of 0·707011 (Valencio *et al.*, 2003) as the contaminant. The bulk partition coefficient for Sr, $D_{Sr} = 3·2$, and the *r* value is 0·009 (*r* = rate of wallrock assimilation/rate of crystal fractionation; DePaolo, 1981).

The geochemical characteristics of the PMVF suggest that the basaltic units and Payún Matrú rocks are genetically related, and have evolved by fractional crystallization to produce the trachytes. The increase in Ba from basalts to intermediate rocks could be related to the absence of alkali feldspar fractionation, and is consistent with the absence of this phase in these rocks. The divergent trend observed in Ba, in the intermediate trachytes, suggests the fractionation of alkali feldspar in some lavas; the strong depletion in Ba in the most silicic trachytes may reflect substantial fractionation of this phase. Biotite fractionation is not as significant as feldspar fractionation, as Rb increases with increasing silica (Fig. 7g).

A two-step fractional crystallization (FC) process describes the genesis of most of the Payún Matrú trachytes (Fig. 15); the first step is from basic compositions to those of the silica-poor trachytes, and the second is from these trachytes to the silica-rich trachytes (not the most radiogenic ones). The small contribution of an upper crustal component (*r* = 0·009 in the AFC calculation) allows an approximation to form the evolved trachytes by FC processes only. For the first step, mass-balance (linear least-squares adjustment) and Rayleigh fractionation calculations (non-linear least-squares adjustment) were performed from sample PM 46 (trachybasalt of the Post-caldera Basalts II unit) to sample PM 13 (trachyte of the Post-caldera Trachyandesites unit; Tables 5–7). The selected mineral compositions in sample PM 46 used for the mass-balance calculations are given in Table 5. For the second step, sample PM 13 was used as the starting composition, and only Rayleigh fractionation calculations were

performed, owing to the lack of mineral composition information. Sample PM 40 (trachyte of the Blocky Trachytes lithofacies, Post-caldera Trachytes unit) was selected as the final composition; this is the sample with the least radiogenic Sr isotope composition of the Post-caldera Trachytes. These calculations show that 60% fractional crystallization of a trachybasalt similar to sample PM 46 can result in 40% of trachytic compositions similar to sample PM 13. The fractionated mineral assemblage consists of 28% plagioclase, 17% clinopyroxene, 8% olivine, 6% Fe–Ti oxides (with $Fe_2O_3/TiO_2 = 80/20$) and 1% apatite (Table 7). Compositions similar to those of the most silicic trachytes (sample PM 40) are reached after further fractionation of alkali feldspar (25%), plagioclase (33%), clinopyroxene (4%) olivine (3%), amphibole (3%), biotite (7%), magnetite (1%) and apatite (2%). Although the proportion of fractionated amphibole and apatite is not high, they may be responsible for the concave-upward REE patterns of the Post-caldera Trachytes and some Pre-caldera Trachytes, given the high partition coefficients for MREE of these minerals. About 12% of the initial mass of basaltic magma is left as residual liquid, after the most silicic trachytic composition is reached. Figure 15 illustrates the two-step fractionation model, as well as an example of a possible mixing scenario between basaltic and trachytic compositions that may result in some of the hybrid samples. The departure of some samples from the FC model liquids in Fig. 15 is interpreted as a result of magma mixing between these end-members compositions, which is consistent with the disequilibrium textures in these lavas (Hernando *et al.*, 2012).
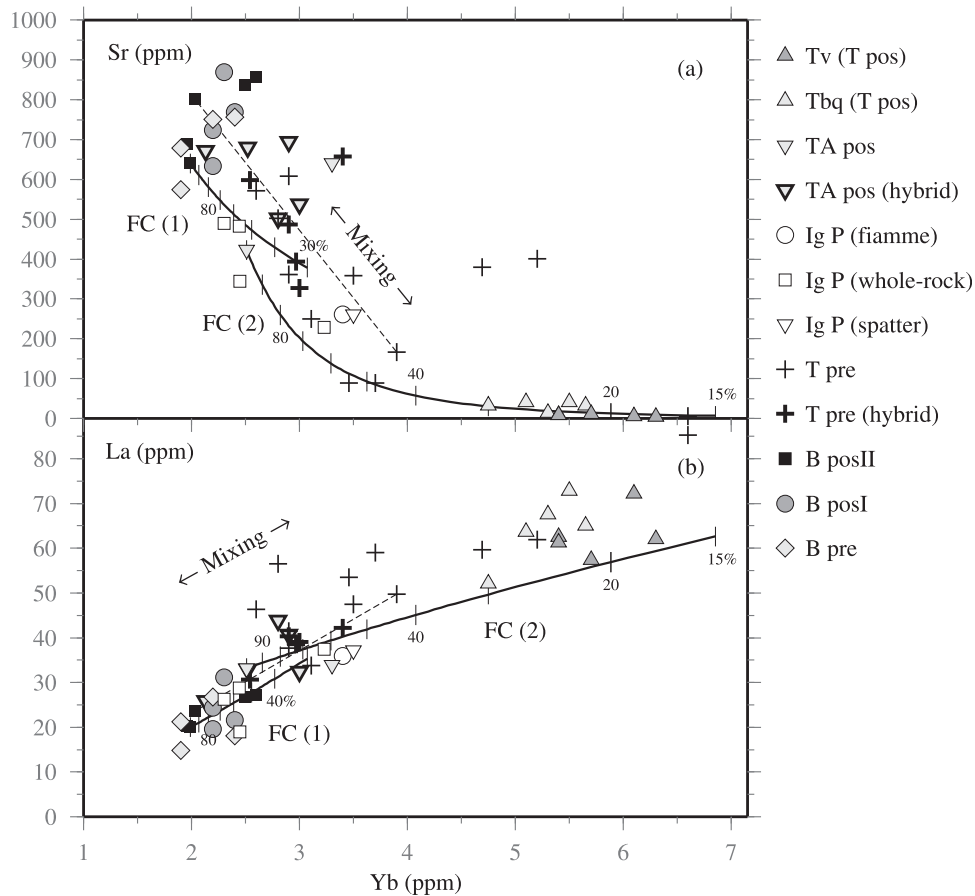
Fig. 15. Variation of Yb vs Sr (a) and La (b) showing the two steps of the Rayleigh fractionation model. FC (1), step one; FC (2), step two. Also shown is a schematic mixing curve between basaltic and trachytic compositions, which may explain some of the hybrid compositions of the Pre-caldera Trachytes and Post-caldera Trachyandesites lavas. The mixing hyperbola is a straight line in such element–element plots (Langmuir *et al.*, 1978).

Zr, Nb and Rb, along with other incompatible elements such as U and Th, show a positive correlation with SiO_2 (not shown) and a spike in their concentrations at high silica contents. One possibility is that these trends are the result of the combined effects of fractional crystallization (without zircon fractionation) and magma mixing processes. The trends produced by only fractional crystallization do not form a straight line, but a concave-upward curve (e.g. Fig. 15a). The effect of magma mixing is to produce compositions that plot along a straight line between the end-member compositions mixed, in element–element plots (Langmuir *et al.*, 1978). If most of the intermediate rocks are the result of magma mixing (between basaltic and silica-poor trachytic compositions) but not the most evolved trachytes, then the result of mixing and fractional crystallization processes would be a trend depicted by a straight line from basalts to silica-poor trachytes. The spike in the incompatible elements from these silica-poor trachytes to the most silicic ones may be due to fractional crystallization processes only.

With regard to the variations observed in $(La/Yb)_N$ (Fig. 9a), a combination of variable degrees of partial melting of the mantle and FC process could be responsible for the observed trends. Variations in the $(La/Yb)_N$ ratio in lavas of the basaltic fields are relatively small (between 5·4 and 9·7), and may represent small differences in the degree of partial melting of the mantle source. The slight increase in $(La/Yb)_N$ from the basaltic to the intermediate rocks may be due to the effect of relatively large amounts of clinopyroxene and Fe–Ti oxide fractionation. Considering the fractionated mineral assemblage in step one of the FC model, the bulk distribution coefficients (D) for La and Yb (Table 6) are slightly different; D_{La} is ∼0·32 whereas D_{Yb} is ∼0·45. Although both elements behave incompatibly, this difference can produce a small change in La/Yb ratios, increasing La relatively to Yb in the resulting trachytes. The reverse situation occurs in step two of FC modelling, in which the resulting D_{La} and D_{Yb} are 0·43 and 0·33, respectively.

Table 5: Selected mineral compositions used for the step-one mass-balance fractionation model

%	Plagioclase	Clinopyroxene	Olivine
SiO$_2$	50·79	48·09	37·38
TiO$_2$	0·09	1·88	0·13
Al$_2$O$_3$	30·31	6·49	0·03
Fe$_2$O$_3$	0·10	–	–
FeO	–	7·96	22·28
MnO	0·00	0·14	0·34
MgO	0·11	13·17	39·10
CaO	13·75	22·35	0·25
Na$_2$O	3·78	0·56	0·03
K$_2$O	0·23	0·01	0·00
P$_2$O$_5$	–	–	–
Total	99·16	100·65	99·54
	An 66	En 39	Fo 75
	Ab 33	Fs 13	Fa 25

A theoretical composition for oxides and apatite is used in the calculations. The mineral compositions were determined by a JEOL-SUPERPROBE JXA-8600 S electron microprobe using 15 kV accelerating potential, 20·10 nÅ sample current and 10 μm electron beam.

The transition to peralkalinity observed in the most silicic trachytes, particularly in the post-caldera stage, may occur as a result of the effect of plagioclase fractionation, which removes Ca and Al, leaving a liquid rich in Na and K. In weakly peralkaline magmas, crystallization of clinopyroxene may exert an important control on magma peralkalinity, because the crystallization of this phase inhibits the evolution of melts towards a more peralkaline character (Scaillet & Macdonald, 2003). Clinopyroxene is always present in the weakly peralkaline trachytes of Payún Matrú, and thus its stability would prevent the development of marked peralkalinity.

The weakly alkaline and Si-undersaturated basalts evolve towards the weakly oversaturated silica-poor trachytes (such as sample PM 13, Table 3). In the SiO$_2$–NaAlSiO$_4$–KAlSiO$_4$ residual system, the silica-poor trachytes of Payún Matrú are located on the modest temperature 'saddle' on the alkali feldspar join (Fig. 16). The further evolution of these trachytes is towards the silica-oversaturated thermal minimum owing to the location of the samples above the alkali feldspar join, and by means of alkali feldspar fractionation (Fig. 16).

There is a strong inferred bimodality in the PMVF, considering that most of the lavas with intermediate compositions represent hybrid magmas (as well as some trachytes; Hernando *et al.*, 2012). This bimodality is present in other volcanic provinces belonging to the transitional alkaline series, such as Gedemsa volcano in Ethiopia (Peccerillo *et al.*, 2003) and Pantelleria island (Ferla & Meli, 2006), and also in basic intrusions and lava lakes (Marsh, 2002). The process of fractional crystallization of alkali basaltic magmas to produce trachytic magmas results in a paucity of intermediate melts, owing to the increase in the amount of crystallization of different minerals in a narrow range of temperature, and the consequent rapid change in melt composition (Pecerillo *et al.*, 2003, 2007).

The pre-caldera stage of Payún Matrú lasted about 600 kyr, beginning at least 700 kyr ago, and resulted in the construction of a multi-vent shield-shaped edifice. This stage is characterized by a high lithological diversity (Fig. 5). The few ages available for the Pre-caldera Trachytes unit, along with the nature of their outcrop, are not sufficient to assess the geochemical evolution of this early stage. The eruption of the Portezuelo Ignimbrite and the formation of the Payún Matrú caldera occurred around 100 ka [between 148 and 82 ka, according to Germa *et al.* (2010) and this study]. This was followed by an important shift in the composition of the erupted products, changing to basaltic trachyandesite and trachyandesite (Post-caldera Trachyandesites unit). Consistent with the abundant mixing textures, these lavas are interpreted to be the result of mixing of basaltic and trachytic magmas (Hernando *et al.*, 2012). In the youngest unit of Payún Matrú, there is again a marked shift in composition, but to relatively homogeneous silicic–trachytic lavas and proximal pyroclastic fall deposits (Post-caldera Trachytes unit).

GEOPHYSICAL CONSTRAINTS ON THE SOURCE(S) OF THE PMVF MAGMAS

The young age of this volcanic field allows comparison of the inferred magma source with several geophysical studies of the crust and mantle in the western South American margin at PMVF latitudes (Wagner *et al.*, 2005; Gilbert *et al.*, 2006; Yuan *et al.*, 2006; Burd *et al.*, 2008; Aragón *et al.*, 2011). Electrical conductivity studies at PMVF latitudes (36·7°S, between 67°W and 70°W) show the presence of a nearly vertical, high-conductivity zone beneath the volcanic field (Burd *et al.*, 2008). This conductivity anomaly, interpreted as a zone containing fluids and/or partial melts, is rooted at 200 km depth, above the projected Nazca subducted slab, and spreads laterally at shallow depths (Burd *et al.*, 2008).

At 36°S, a subcrustal low-velocity zone 20 km thick and 250 km wide, between 40 and 60 km deep, has been detected below the back-arc volcanic region, and has been interpreted as the possible base of the lithosphere (Gilbert *et al.*, 2006). This interpretation may be reasonable on a more regional scale, because crustal thicknesses in the Andean back-arc, as interpreted from seismic velocities at

Table 6: Published values of mineral–melt partition coefficients (K_D) used for Rayleigh fractionation modeling

Step one of fractional crystallization model, from trachybasalt to silica-poor trachyte

	Pl (An 65)	Cpx	Ol	Mgt	Ap
Rb	0·13[1]	0·13[1]	0·0084[2]	0·11[5]	0·56[6]
Sr	2·70[1]	0·16[1]	0·02[1]	0·16[6]	1·67[6]
Ba	0·56[1]	0·04[1]	0·03[1]	0·14[6]	0·95[6]
La	0·20[1]	0·288[3]	0·03[1]	0·10[5]	8·6[8]
Ce	0·023[2]	0·202[3]	0·0020[4]	0·20[7]	11·2[8]
Nd	0·023[2]	0·888[3]	0·0023[4]	0·25[7]	14·0[8]
Sm	0·024[2]	0·978[3]	0·0108[4]	0·30[7]	14·6[8]
Eu	0·5[1]	0·925[3]	0·03[1]	0·09[5]	9·6[8]
Gd	0·066[2]	0·889[3]	0·0168[4]	0·30[7]	15·8[8]
Tb	0·11[1]	0·73[1]	0·03[1]	0·55[6]	15·4[8]
Dy	0·055[2]	0·960[3]	0·0263[4]	0·30[7]	8·9[9]
Yb	0·030[2]	0·990[3]	0·0313[4]	0·25[7]	8·1[8]
Lu	0·037[2]	0·968[3]	0·0383[4]	0·75[6]	3·8[9]
Hf	0·05[1]	0·1094[4]	0·04[1]	0·16[5]	0·64[6]
Ta	0·04[1]	0·04[1]	0·03[1]	0·23[5]	0·09[6]

Step two of fractional crystallization model, from silica-poor trachyte to silica-rich trachyte

	Kfsp (~Or 41)	Pl (~An 40)	Ol	Cpx	Amp	Bt	Mgt	Ap
Rb	0·32[10]	0·2[6]	0·08[5]	0·015[10]	0·14[5]	1·35[12]	0·01[5]	0·4[14]
Sr	2·3[10]	4·41[6]	0·053[10]	0·25[10]	0·58[13]	0·2[12]	–	8[14]
Ba	3·409[10]	1·08[6]	0·023[10]	0·009[10]	0·15[11]	4·04[12]	0·07[11]	0·3[11]
La	0·052[10]	0·16[11]	0·06[10]	0·296[10]	0·54[11]	0·17[12]	0·29[11]	21·7[11]
Ce	0·039[10]	0·12[11]	0·08[10]	0·458[10]	0·98[11]	–	0·35[11]	25·8[11]
Nd	0·026[10]	0·07[11]	0·085[10]	0·769[10]	2·1[11]	–	–	29·0[11]
Sm	0·028[10]	0·061[11]	0·087[10]	0·87[10]	2·99[11]	–	0·55[11]	31·4[11]
Eu	1·261[10]	0·79[11]	0·104[10]	1·2[10]	2·88[11]	0·56[12]	0·53[11]	25·2[11]
Tb	0·02[10]	0·05[11]	0·127[10]	0·48[12]	4·8[11]	0·24[12]	0·5[11]	34·0[11]
Dy	0·025[10]	0·09[11]	0·164[10]	0·764[10]	4·3[11]	–	–	24·0[11]
Yb	0·028[10]	0·026[11]	0·26[10]	0·831[10]	2·29[11]	–	0·26[11]	12·3[11]
Lu	0·11[6]	0·1[11]	–	–	2·3[11]	–	0·6[11]	12·0[11]
Hf	0·009[10]	0·064[11]	0·011[10]	0·395[10]	0·76[11]	0·13[12]	0·25[14]	0·4[11]
Ta	0·12[6]	0·027[11]	0·14[5]	0·24[12]	0·56[11]	0·74[12]	2·2[14]	0·25[11]

Pl, plagioclase; Cpx, clinopyroxene; Ol, olivine; Mgt, magnetite; Ap, apatite; Kfsp, alkali feldspar; Amp, amphibole; Bt, biotite. [1]Villemant *et al*. (1981); [2]Schnetzler & Philpotts (1970); [3]Shimizu (1980); [4]Fujimaki *et al*. (1984); [5]Lemarchand *et al*. (1987); [6]Caroff *et al*. (1993); [7]Reid (1983); [8]Paster *et al*. (1974); [9]Watson & Green (1981); [10]Larsen (1979); [11]Luhr *et al*. (1984); [12]Villemant (1988); [13]Nagasawa (1973); [14]Mahood & Stimac (1990).

around 39°S (~300 km south of the PMVF), are 30–35 km, and increase in the volcanic arc zone to 40 km (Wagner *et al*., 2005; Yuan *et al*., 2006). Although the crustal thickness reported by Yuan *et al*. (2006) is relatively far from the PMVF, it is consistent with the crustal thickness inferred by Gilbert *et al*. (2006) at PMVF latitudes.

The presence of the low-velocity zone in the back-arc area would imply the presence of an attenuated lithosphere at PMVF latitudes.

Tomographic models of the mantle of southern South America, based on P-wave velocity perturbations, show the presence of a normal subduction zone at Payenia

Table 7: Results of least-squares mass-balance fractionation and Rayleigh fractionation for PMVF rocks

Step one of the fractional crystallization model

Mass balance

PM $46 = 0.40$ PM $13 + 0.28$ Pl (An 66) $+ 0.17$ Cpx (En 39) $+ 0.08$ Ol (Fo 75) $+ 0.06$ Fe–Ti oxides $+ 0.01$ Ap

	SiO_2	TiO_2	Al_2O_3	Fe_2O_3	MnO	MgO	CaO	Na_2O	K_2O	P_2O_5	$\sum R^2$
Meas.	49·73	2·00	16·81	10·29	0·15	5·79	9·41	3·79	1·58	0·44	
Calc.	49·75	2·01	16·83	10·28	0·10	5·79	9·38	3·53	1·66	0·48	
Res.	−0·02	−0·01	−0·02	0·02	0·05	0·00	0·03	0·26	−0·08	−0·04	0·08

Rayleigh fractionation

	Rb	Sr	Ba	La	Ce	Nd	Sm	Eu	Gd	Tb	Dy	Yb	Lu	Hf
Meas.	93	423	768	33·20	72·30	31·70	6·39	2·13	5·76	0·86	4·78	2·51	0·38	10·80
Calc.	57·54	429·39	729·14	30·82	64·78	27·14	5·79	2·03	5·53	0·92	6·14	2·77	0·45	9·81
D	0·13	1·44	0·34	0·53	0·52	0·83	0·89	0·89	0·93	0·92	0·68	0·64	0·51	0·10

Step two of the fractional crystallization model

Rayleigh fractionation

	Rb	Sr	Ba	La	Ce	Nd	Sm	Eu	Tb	Dy	Yb	Lu	Hf	Ta
Meas.	187	33	201	52·10	96·00	34·50	6·39	0·65	1·00	6·15	4·75	0·71	18·50	6·52
Calc.	196·77	32·56	197·86	49·12	96·75	37·52	6·67	0·96	0·77	5·73	4·67	0·69	28·87	10·53
D	0·36	3·19	2·16	0·67	0·75	0·86	0·96	1·68	1·09	0·85	0·47	0·48	0·16	0·22

D, bulk partition coefficient for each step of fractionation, calculated using published partition coefficients (Table 6). For both the mass-balance and Rayleigh fractionation modelling, the measured compositions were weighted according to the uncertainties of the chemical analyses (detection limits). The parameters estimated in the mass-balance adjustment were introduced as *a priori* values for the Rayleigh fractionation modelling. The uncertainties in the partition coefficients could propagate to the estimated trace element composition.

latitudes and, to the north, the Pampean flat slab subduction zone (27–33°S) (Fig. 17). The resolution of the tomography decreases with depth (Electronic Appendix 1) and small details cannot be detected, but, nevertheless, it can be used as a crude approximation for the location of the subducted Nazca slab. Although the PMVF is located in a normal subduction zone (i.e. with a dip angle of the subducted oceanic plate of ∼30°), it is relatively close to the northern flat slab subduction segment. The subducted oceanic slab (positive velocity perturbation in the mantle tomography of Fig. 17a) is detected at around 200 km depth below the PMVF, and it is interrupted slightly east of the volcanic field. Figure 18 shows the South American margin profile at 36·5°S and the schematic base of crust and lithosphere as well as the oceanic subducted slab, as

inferred from geophysical studies. At 39°S, the subducted Nazca oceanic slab has a mean dip of 25° between 50 and 100 km, and a mean dip of 40° from 100 to 200 km, as inferred from earthquakes in the Wadati–Benioff zone and seismic reflections, and thus the projected slab would be at 300 km or more below the PMVF (Yuan *et al.*, 2006). These dips are slightly higher than those observed in the tomographic section of Fig. 17a, where the oceanic slab is detected above 300 km depth.

AN INTEGRATED MODEL

The relatively thin lithosphere present in the back-arc area of the PMVF (Gilbert *et al.*, 2006) is consistent with the proposed spinel lherzolite magma source, as inferred from
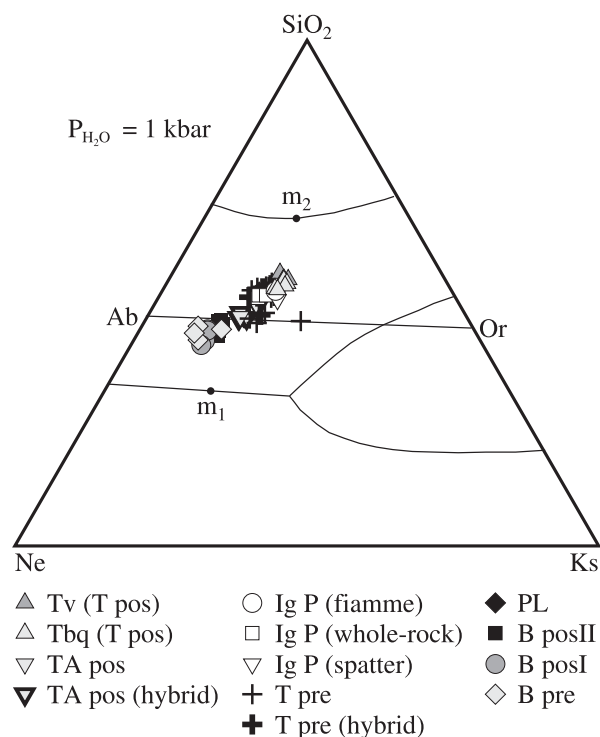
Fig. 16. SiO_2–$NaAlSiO_4$ (Ne)–$KAlSiO_4$ (Ks) residual system showing all samples of the PMVF. Phase boundaries (P_{H_2O} 1 kbar) according to Hamilton & MacKenzie (1965). m_1, silica-undersaturated thermal minimum; m_2, silica-oversaturated thermal minimum. Although this diagram is traditionally used for silicic compositions, here the basalts are also plotted to illustrate the characteristics of the whole volcanic field. Because mafic minerals are an important component of basaltic magmas, the residual system does not fully represent these magmas. The general evolutionary trend of Payún Matrú rocks is towards the silica-oversaturated thermal minimum.

the geochemical data. The transition from spinel to garnet peridotite is variable and depends not only on pressure, but also on mantle temperature. If there is a positive thermal anomaly, the transition from spinel to garnet is deeper than in colder mantle zones. Gudnason et al. (2012) proposed the presence of a mantle plume below the PMVF, which could produce the electrical conductivity anomaly observed by Burd et al. (2008). An alternative explanation is that there is a localized upwelling of the uppermost asthenospheric mantle, which partially melts in its upper portion as a result of adiabatic decompression.

Slab fluids do not appear to be involved in the generation of magmas erupted in the PMVF (Figs 10e and 12). This could be because the Nazca plate is already dehydrated under the back-arc region, or it may be because the subducted oceanic plate is not present below the volcanic field, a possible situation considering the available geophysical data (Fig. 17a). The transition from the Miocene flat slab period to the normal subduction period that occurred at around 5 Ma (Kay, 2004; Kay et al.,

2006a) would probably produce a detachment between the flat and normal slabs segments. This is observed in the seismic anomaly pattern at 100 km depth below the volcanic arc, which is thought to represent the possible remains of the oceanic slab fragment subducted during the Miocene flat slab period (Yuan et al., 2006), although this seismic anomaly is detected at 39°S, which is south of the proposed Miocene flat slab segment. If detachment between the flat and normal subduction segments of the Nazca plate occurred near the Chile–Perú trench, then the present interruption of the Nazca slab slightly east of the PMVF may reflect the relatively short time since the transition from the Miocene flat slab regime to the Pliocene–Quaternary normal subduction regime, given the actual mean convergence rate of 65 mm a^{-1} (Angermann et al., 1999). This would produce a lack of slab influence in the PMVF magmas and an intraplate affinity, owing to mantle upwelling and adiabatic decompression, producing partial melting of the asthenosphere.

CONCLUSIONS

The PMVF is part of the back-arc Payenia Basaltic Province and is contemporaneous with the Andean volcanic arc located around 150 km to the west. In the PMVF, basaltic fields of basaltic and trachybasaltic composition coexist with trachytic polygenetic volcanoes (Payún Matrú and Payún Liso). The age of the PMVF is Pleistocene–Holocene; the oldest dated lava is 700 kyr old (Payún Matrú) and the youngest is 2 kyr old (basaltic fields).

The PMVF rocks have an intraplate affinity without the influence of slab-derived fluids. The basaltic units have geochemical and isotopic similarity to OIB, and do not represent primary magmas. The basaltic magmas were presumably generated in the asthenosphere, within the spinel stability field, and erupted without significant interaction with the continental lithosphere. Magma generation could be linked to passive mantle upwelling, which may have been favoured by the interruption of the subducted oceanic slab under the PMVF.

The basaltic and trachytic rocks are genetically related, and the evolution of PMVF magmas can be explained by a three-stage fractional crystallization process: first, from primary basaltic magmas to basalts of Pre- and Post-caldera units; second, from these evolved basalts to the silica-poor trachytes (Portezuelo Ignimbrite and some Pre-caldera Trachytes); third, a further fractionation stage that produced the evolved silica-rich trachytes, represented by the Post-caldera Trachytes unit and scarce Pre-caldera Trachytes. A small amount of upper crustal contamination is present in some of the youngest and most evolved trachytic lavas.
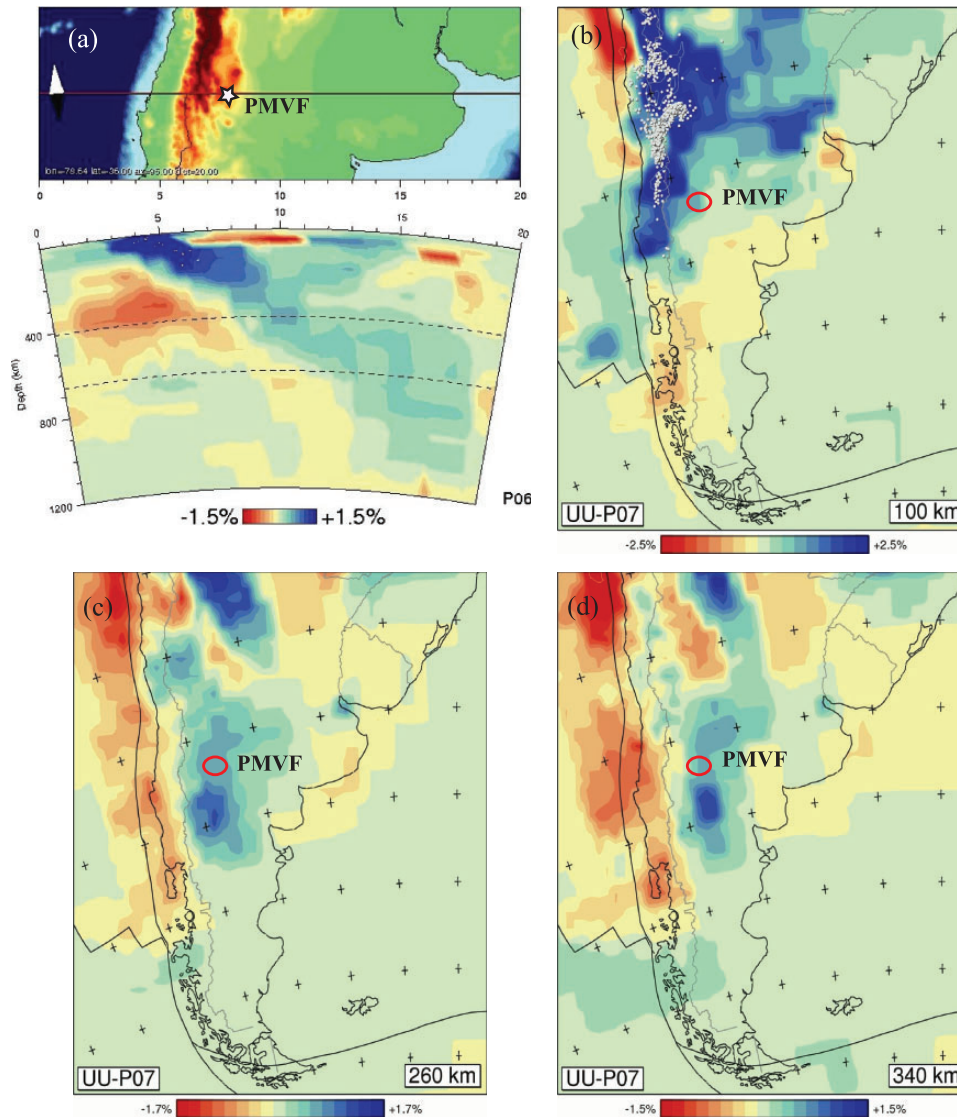
Fig. 17. Global P-wave speed tomography model (UU-P07) is from the PhD thesis of Amaru (2007). It is important to note that this model was labelled P06 in the original thesis but has subsequently been labelled UU-P07 in a number of publications (van der Meer *et al.*, 2010, 2012; Schellart & Spakman, 2012; van Benthem *et al.*, 2013). This model is a successor to the BSE model of Bijwaard *et al.* (1998) and uses a similar method. The lower mantle part of the model has been discussed by van der Meer *et al.* (2010). The reference model used for the tomography is ak135 of Kennett *et al.* (1995). The percentages displayed are relative to the P-wave speed reference values at all depths, expressed as perturbation in per cent. (a) Profile at 36·5°S, showing the interruption of the subducted slab below and slightly east of the PMVF. (b), (c) and (d) show P-wave velocity maps at depths of 100, 260 and 340 km respectively, clearly showing the high-velocity subducted slab below the volcanic arc at 100 km and its interruption at greater depths in the back-arc area. The earthquakes plotted as white dots (1964–2000) in (b) are selected from an updated version of the EHB dataset (Engdahl *et al.*, 1998).

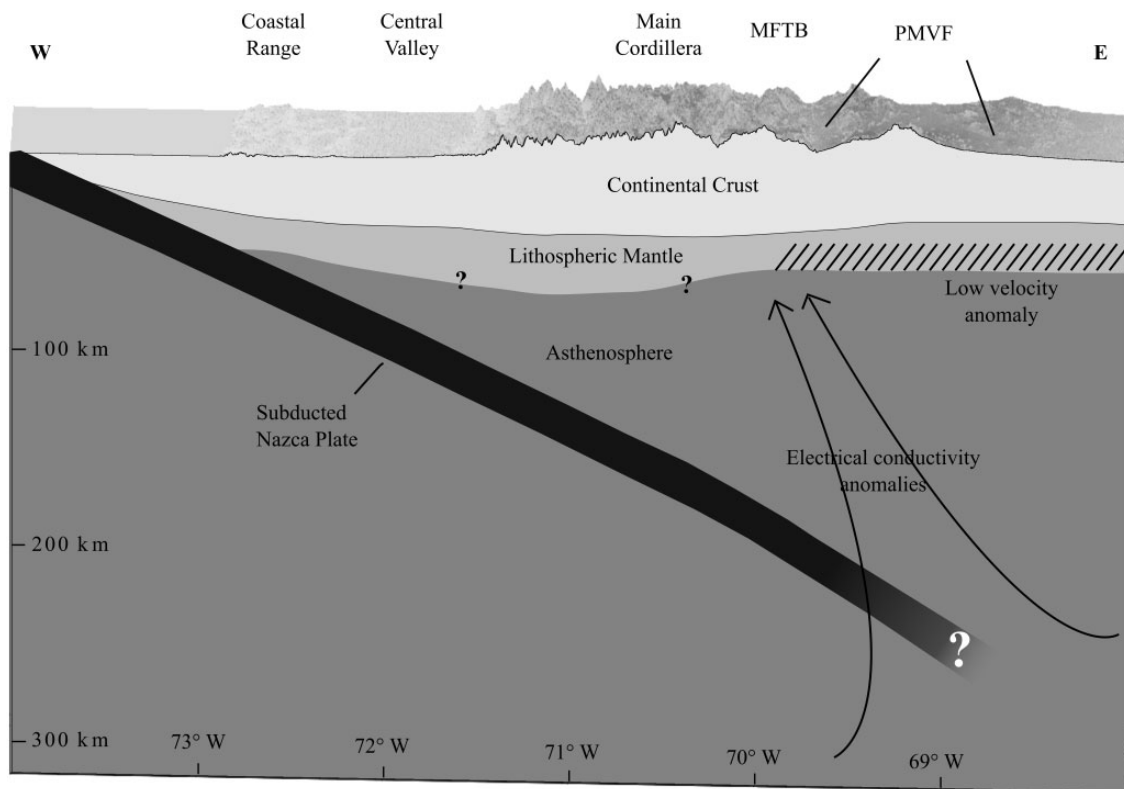**Fig. 18.** Schematic west–east profile of the western margin of South America at 36°25′S with topographic vertical exaggeration of around six. The subducted Nazca plate has been drawn according to the mantle profile shown in Fig. 17a, where it is observed that the slab could be interrupted to the east of the PMVF, as indicated by the question mark. The thickness of crust and mantle in the arc and back-arc zone are as inferred by Wagner *et al.* (2005) and Gilbert *et al.* (2006). The diagonally shaded zone corresponds to seismic anomalies in the back-arc area, with a zone of low velocity between 40 and 60 km depth, interpreted as the possible base of the lithosphere (Gilbert *et al.*, 2006). Arrows show the schematic position of electrical conductivity anomalies below the PMVF (Burd *et al.*, 2008). MFTB, Malargüe fold and thrust belt (Miocene).

FUNDING

SUPPLEMENTARY DATA

Supplementary data for this paper are available at *Journal of Petrology* online.

REFERENCES

Amaru, M. L. (2007). Global travel time tomography with 3-D reference models. PhD thesis, Utrecht University, Utrecht.

Angermann, D., Klotz, J. & Reigber, C. (1999). Space-geodetic estimation of the Nazca–South America Euler vector. *Earth and Planetary Science Letters* **171**, 329–334.

Aragón, E., D'Eramo, F., Castro, A., Pinotti, L., Brunelli, D., Rabbia, O., Rivalenti, G., Varela, R., Spakman, W., Demartis, M., Cavarozzi, C. E., Aguilera, Y. E., Mazzucchelli, M. & Ribot, A. (2011). Tectono-magmatic response to major convergence changes in the North Patagonian suprasubduction system; the Paleogene subduction–transcurrent plate margin transition. *Tectonophysics* **509**, 218–237.

Baier, J., Audétat, A. & Keppler, H. (2007). The origin of the negative niobium tantalum anomaly in subduction zone magmas. *Earth and Planetary Science Letters* **267**, 290–300.

Bermúdez, A. & Delpino, D. (1989). La provincia basáltica andino cuyana. *Revista de la Asociación Geológica Argentina* **44**, 35–55.

Bermúdez, A., Delpino, D., Frey, F. & Saal, A. (1993). Los basaltos de retroarco extraandinos. In: Ramos, V. A. (ed.) *Geología y Recursos Naturales de Mendoza. Relatorio I* **13**, 161–172.

Bertotto, G. W., Cingolani, C. A. & Bjerg, E. A. (2009). Geochemical variations in Cenozoic back-arc basalts at the border of La Pampa and Mendoza provinces, Argentina. *Journal of South American Earth Sciences* **28**, 360–373.

Bijwaard, H. & Spakman, W. (2000). Non-linear global P-wave tomography by iterated linearized inversion. *Geophysical Journal International* **141**, 71–82.

Bijwaard, H., Spakman, W. & Engdahl, E.R. (1998). Closing the gap between regional and global travel time tomography. *Journal of Geophysical Research* **103(B12)**, 55–78.

Burd, A., Booker, J. R., Pomposiello, M., Favetto, A., Larsen, J., Giordanengo, G. & Orozco Bernal, L. (2008). Electrical conductivity beneath the Payún Matrú Volcanic Field in the Andean backarc of Argentina near 36.5°S: Insights into the magma source. In: *7th International Symposium on Andean Geodynamics (Nice), Extended Abstracts*. Institut de Recherche pour le Développement (IRD), pp. 90–93.

Cagnoni, M. C., Ramos, A. M., Valencio, S. A., Panarello, H. O., Armella, C. & Cabaleri, N. G. (2006). $\delta^{13}C$, $\delta^{18}O$ and $^{87}Sr/^{86}Sr$ of early Callovian limestones from Cuenca Neuquina, Argentina. In: Gaucher, C. & Bossi, J. (eds) In: *V South American Symposium on Isotope Geology (Punta del Este), Short Papers*, pp. 230–234.

Caroff, M., Maury, R. C., Leterrier, J., Joron, J. L., Cotten, J. & Guille, G. (1993). Trace element behavior in the alkali basalt–comenditic trachyte series from Mururoa Atoll, French Polynesia. *Lithos* **30**, 1–22.

DePaolo, D. J. (1981). Trace element and isotopic effects of combined wallrock assimilation and fractional crystallization. *Earth and Planetary Science Letters* **53**, 189–202.

Engdahl, E. R., van der Hilst, R. & Buland, R. (1998). Global teleseismic earthquake relocation with improved travel times and procedures for depth determination. *Bulletin of the Seismological Society of America* **88(3)**, 722–743.

Espáñon, V. R., Honda, M. & Chivas, A. R. (2013). Cosmogenic noble gas dating of young basaltic lavas from southern Mendoza, Argentina. *Quaternary Geochronology* (in press).

Farmer, G. L. (2003). Continental basaltic rocks. In: Holland, H. D. & Turekian, K. K. (eds) *Treatise on Geochemistry*. Pergamon, pp. 1–39.

Ferla, P. & Meli, C. (2006). Evidence of magma mixing in the Daly Gap of alkaline suites: A case study from the enclaves of Pantelleria (Italy). *Journal of Petrology* **47(8)**, 1467–1507.

Fitton, J. G., James, D. & Leeman, W. P. (1991). Basic magmatism associated with Late Cenozoic extension in the Western United States: Compositional variations in space and time. *Journal of Geophysical Research* **96(B8)**, 13693–13711.

Folguera, A., Naranjo, J. A., Orihashi, Y., Sumino, H. & Nagao, K. (2009). Retroarc volcanism in the northern San Rafael Block (34°–35°30′S), southern Central Andes: Occurrence, age, and tectonic setting. *Journal of Volcanology and Geothermal Research* **186**, 169–185.

Fujimaki, H., Tatsumoto, M. & Aoki, K. I. (1984). Partition coefficients of Hf, Zr and REE between phenocrysts and groundmass. *Journal of Geophysical Research* **89**, 662–672.

Germa, A., Quidelleur, X., Gillot, P. Y. & Tchilinguirian, P. (2010). Volcanic evolution of the back-arc Pleistocene Payun Matru volcanic field (Argentina). *Journal of South American Earth Sciences* **29**, 717–730.

Gibson, S. A., Thompson, R. N., Leat, P. T., Dickin, A. P., Morrison, M. A., Hendry, G. L. & Mitchell, J. G. (1992). Asthenosphere-derived magmatism in the Rio Grande rift, western USA: implications for continental break-up. In: Storey, B. C., Alabaster, T. & Pankhurst, R. J. (eds) *Magmatism and the Causes of Continental Break-up. Geological Society, London, Special Publications* **68**, 61–89.

Gilbert, H., Beck, S. & Zandt, G. (2006). Lithospheric and upper mantle structure of central Chile and Argentina. *Geophysical Journal International* **165**, 383–398.

González Díaz, E. (1972). *Descripción geológica de la Hoja 30^d, Payún Matrú, Boletín 130, Dirección Nacional de Geología y Minería*. Buenos Aires: Ministerio de Industria y Minería.

Groeber, P. (1946). Observaciones Geológicas a lo Largo del Meridiano 70: 1. Hoja Chos Malal. *Revista de la Asociación Geológica Argentina* **1(3)**, 177–208.

Gudnason, J., Holm, P. M., Søager, N. & Llambías, E. J. (2012). Geochronology of the late Pliocene to recent volcanic activity in the Payenia back-arc volcanic province, Mendoza, Argentina. *Journal of South American Earth Sciences* **37**, 191–201.

Hamilton, D. L. & MacKenzie, W. S. (1965). Phase equilibrium studies in the system NaAlSiO$_4$ (nepheline)–KAlSiO$_4$ (kalsilite)–SiO$_2$–H$_2$O. *Mineralogical Magazine* **34**, 214–231.

Hernando, I. R., Llambías, E. J., González, P. D. & Sato, K. (2012). Volcanic stratigraphy and evidence of magma mixing in the Quaternary Payún Matrú volcano, Andean backarc in western Argentina. *Andean Geology* **39(1)**, 158–179.

Inbar, M. & Risso, C. (2001). Holocene yardangs in volcanic terrains in the southern Andes. *Earth Surface Processes and Landforms* **26**, 657–666.

Irvine, T. N. & Baragar, W. R. A. (1971). A guide to the chemical classification of the common volcanic rocks. *Canadian Journal of Earth Sciences* **8**, 523–548.

Jicha, B. R., Coombs, M. L., Calvert, A. T. & Singer, B. S. (2012). Geology and $^{40}Ar/^{39}Ar$ geochronology of the medium- to high-K Tanaga volcanic cluster, western Aleutians. *Geological Society of America Bulletin* **124(5–6)**, 842–856.

Kalsbeek, F. & Frei, R. (2006). The Mezoproterozoic Midsommersø dolerites and associated high–silica intrusions, North Greenland: crustal melting, contamination and hydrothermal alteration. *Contributions to Mineralogy and Petrology* **152(1)**, 89–110.

Kay, S. M. (2002). Magmatic sources, tectonic setting and causes of Tertiary to recent Patagonian plateau magmatism (36°S to 52°S latitude). In: Cingolani, C. A., Cabaleri, N., Linares, E., López de Luchi, M. G., Ostera, H. A. & Panarello, H. O. (eds) *Proceedings XV Congreso Geológico Argentino*, Asociación Geológica Argentina, Extended Abstracts, Calafate, pp. 95–10.

Kay, S. M., Gorring, M. & Ramos, V. A. (2004). Magmatic sources, setting and causes of Eocene to recent Patagonian plateau magmatism (36°S to 52°S latitude). *Revista de la Asociación Geológica Argentina* **59(4)**, 556–568.

Kay, S. M., Burns, W. M., Copeland, P. & Mancilla, O. (2006*a*). Upper Cretaceous to Holocene magmatism and evidence for transient Miocene shallowing of the Andean subduction zone under the northern Neuquén Basin. In: Kay, S. M. & Ramos, V. A. (eds) *Evolution of an Andean Margin: A Tectonic and Magmatic View from the Andes to the Neuquén Basin (35°–39°S Latitude). Geological Society of America, Special Papers* **407**, 19–60.

Kay, S. M., Mancilla, O. & Copeland, P. (2006*b*). Evolution of the late Miocene Chachahuén volcanic complex at 37°S over a transient shallow subduction zone under the Neuquén Andes. In: Kay, S. M. & Ramos, V. A. (eds) *Evolution of an Andean Margin: A Tectonic and Magmatic View from the Andes to the Neuquén Basin (35°–39°S Latitude). Geological Society of America, Special Papers* **407**, 215–246.

Kennett, B. L. N., Engdahl, E. R. & Buland, R. (1995). Constraints on seismic velocities in the Earth from travel times. *Geophysical Journal International* **122(1)**, 108–124.

Langmuir, C. H., Vocke, R. D., Jr, Hanson, G. N. & Hart, S. R. (1978). A general mixing equation with applications to Icelandic basalts. *Earth and Planetary Science Letters* **37**, 380–392.

Larsen, L. M. (1979). Distribution of REE and other trace-elements between phenocrysts and peralkaline undersaturated magmas, exemplified by rocks from the Gardar Igneous Province, south Greenland. *Lithos* **12(4)**, 303–315.

Leat, P. T., Thompson, R. N., Morrison, M. A., Hendry, G. L. & Dickin, A. P. (1990). Geochemistry of mafic lavas in the early Rio Grande Rift, Yarmony Mountain, Colorado, U.S.A. *Chemical Geology* **81**, 23–43.

Lemarchand, F., Benoit, V. & Calais, G. (1987). Trace element distribution coefficients in alkaline series. *Geochimica et Cosmochimica Acta* **51**, 1071–1081.

Lipman, P. W. (2000). Calderas. In: Sigurdsson, H. (ed.) *Encyclopedia of Volcanoes*. Academic Press, pp. 643–662.

Llambías, E. J. (1966). Geología y petrología del volcán Payún Matrú. *Acta Geológica Lilloana* **8**, 265–315.

Llambías, E. J., Bertotto, G. W., Risso, C. & Hernando, I. R. (2010). El volcanismo cuaternario en el retroarco de Payenia: una revisión. *Revista de la Asociación Geológica Argentina* **67(2)**, 278–300.

Lofgren, G. (1970). Experimental devitrification rate of rhyolite glass. *Geological Society of America Bulletin* **81**, 553–560.

Lo Forte, G. L., Ortí, F. & Rosell, L. (2005). Isotopic characterization of Jurassic evaporites. Aconcagua–Neuquén Basin, Argentina. *Geológica Acta* **3**, 155–161.

Luhr, J. F., Carmichael, I. S. E. & Varekamp, J. C. (1984). The 1982 eruptions of El Chichón volcano, Chiapas, Mexico: mineralogy and petrology of the anhydrite-bearing pumices. *Journal of Volcanology and Geothermal Research* **23**, 69–108.

Macdonald, R. (1974). Nomenclature and petrochemistry of the peralkaline oversaturated extrusive rocks. *Bulletin Volcanologique* **38**, 498–516.

Mahood, G. A. & Stimac, J. A. (1990). Trace-element partitioning in pantellerites and trachytes. *Geochimica et Cosmochimica Acta* **54**, 2257–2276.

Marchetti, D., Cerling, T., Evenson, E., Gosse, K. J. & Martinez, O. (2006). Cosmogenic exposure ages of lava flows that temporarily dammed the Río Grande and Río Salado, Mendoza province, Argentina. In: *Backbone of the Americas—Patagonia to Alaska. Geological Society of America, Special Meeting*, Abstracts with programs **2**, 66 p.

Marsh, B. D. (2002). On bimodal differentiation by solidification front instability in basaltic magmas, part 1: Basic mechanics. *Geochimica et Cosmochimica Acta* **66(12)**, 2211–2229.

Mattsson, H. & Oskarsson, N. (2005). Petrogenesis of alkaline basalts at the tip of a propagating rift: Evidence from the Heimaey volcanic centre, south Iceland. *Journal of Volcanology and Geothermal Research* **147**, 245–267.

Nagasawa, H. (1973). Rare-earth distribution in alkali rocks from Oki-Dogo Island, Japan. *Contributions to Mineralogy and Petrology* **39**, 301–308.

Niu, Y. & O'Hara, M. J. (2003). Origin of ocean island basalts: A new perspective from petrology, geochemistry, and mineral physics considerations. *Journal of Geophysical Research* **108**(**B4**), doi: 10.1029/2002JB002048.

Parfitt, E. & Wilson, L. (2008). *Fundamentals of Physical Volcanology*. Oxford: Blackwell.

Paster, T. P., Schauwecker, D. S. & Haskin, L. A. (1974). The behavior of some trace elements during solidification of the Skaergaard layered series. *Geochimica et Cosmochimica Acta* **38(10)**, 1549–1577.

Pearce, J. A. (1982). Trace element characteristics of lavas from destructive plate boundaries. In: Thorpe, R. S. (ed.) *Andesites*. John Wiley, pp. 525–548.

Pearce, J. A. (1983). Role of the sub-continental lithosphere in magma genesis at active continental margins. In: Hawkesworth, C. J. & Norry, M. J. (eds) *Continental Basalts and Mantle Xenoliths*. Shiva, pp. 230–249.

Peccerillo, A., Barberio, M. R., Yirgu, G., Ayalew, D., Barbieri, M. & Wu, T. W. (2003). Relationship between mafic and peralkaline silicic magmatism in continental rift settings: a petrological, geochemical and isotopic study of the Gedemsa Volcano, Central Ethiopian Rift. *Journal of Petrology* **44(11)**, 2003–2032.

Peccerillo, A., Donati, C., Santo, A. P., Orlando, A., Yirgu, A. & Ayalew, D. (2007). Petrogenesis of silicic peralkaline rocks in the Ethiopian rift: Geochemical evidence and volcanological implications. *Journal of African Earth Sciences* **48**, 161–173.

Pilet, S., Hernandez, J., Sylvester, P. & Poujol, M. (2005). The metasomatic alternative for ocean island basalt chemical heterogeneity. *Earth and Planetary Science Letters* **236**, 148–166.

Pilet, S., Baker, M. B. & Stolper, E. M. (2008). Metasomatized lithosphere and the origin of alkaline lavas. *Science* **320**, 916–919.

Pilet, S., Baker, M. B., Müntener, O. & Stolper, E. M. (2011). Monte Carlo simulations of metasomatic enrichment in the lithosphere and implications for the source of alkaline basalts. *Journal of Petrology* **52(7–8)**, 1415–1442.

Polanski, J. (1954). Rasgos geomorfológicos del territorio de la provincia de Mendoza. *Cuadernos de Estudio e Investigación, Instituto de Investigaciones Económicas y Tecnológicas* **4**, 4–10.

Ramos, V. A. & Folguera, A. (2005). Tectonic evolution of the Andes of Neuquén: constraints derived from the magmatic arc and foreland deformation. In: Veiga, G. D., Spalletti, L. A., Howell, J. A. & Schwarz, E. (eds) *The Neuquen Basin, Argentina: a Case Study in Sequence Stratigraphy and Basin Dynamics. Geological Society, London, Special Publications* **252**, 15–35.

Ramos, V. A. & Folguera, A. (2011). Payenia volcanic province in the Southern Andes: An appraisal of an exceptional Quaternary tectonic setting. *Journal of Volcanology and Geothermal Research* **201**, 53–64.

Ramos, V. A. & Kay, S. M. (2006). Overview of the tectonic evolution of the southern Central Andes of Mendoza and Neuquén (35°–39°S latitude). In: Kay, S. M. & Ramos, V. A. (eds) *Evolution of an Andean Margin: A Tectonic and Magmatic View from the Andes to the Neuquén Basin (35°–39°S lat.). Geological Society of America, Special Papers* **407**, 1–17.

Reid, F. (1983). Origin of the rhyolitic rocks of the Taupo Volcanic Zone, New Zealand. *Journal of Volcanology and Geothermal Research* **15(4)**, 315–338.

Scaillet, B. & Macdonald, R. (2003). Experimental constraints on the relationships between peralkaline rhyolites of the Kenya Rift Valley. *Journal of Petrology* **44(10)**, 1867–1894.

Schellart, W. P. & Spakman, W. (2012). Mantle constraints on the plate tectonic evolution of the Tonga–Kermadec–Hikurangi subduction zone and the South Fiji Basin region. *Australian Journal of Earth Science* **59(6)**, 933–952.

Schnetzler, C. C. & Philpotts, J. A. (1970). Partition coefficients of rare-earth elements between igneous matrix material and rock-forming mineral phenocrysts; II. *Geochimica et Cosmochimica Acta* **34(3)**, 331–340.

Shimizu, H. (1980). Experimental study on rare-earth element partitioning in minerals formed at 20 and 30 kb for basaltic systems. *Geochemical Journal* **14(4)**, 185–202.

Stern, C. R., Frey, F. A., Futa, K., Zartman, R. E., Peng, Z. & Kyser, T. K. (1990). Trace element and Sr, Nd, Pb, and O isotopic composition of Pliocene and Quaternary alkali basalts of the Patagonian Plateau lavas of southernmost South America. *Contributions to Mineralogy and Petrology* **104**, 294–308.

Sun, S. & McDonough, W. F. (1989). Chemical and isotopic systematics of oceanic basalts: implications for mantle composition and processes. In: Saunders, A. D. & Norry, M. J. (eds) *Magmatism in the Ocean Basins. Geological Society, London, Special Publications* **42**, 313–345.

Thompson, R. N. (1984). Dispatches from the basalt front. 1. Experiments. *Proceedings of the Geologists' Association* **95**, 249–262.

Timm, C., Hoernle, K., Werner, R., Hauff, F., van den Bogaard, P., White, J., Mortimer, N. & Garbe-Schönberg, D. (2010). Temporal and geochemical evolution of the Cenozoic intraplate volcanism of Zealandia. *Earth-Science Reviews* **98**, 38–64.

Tormey, D. R., Hickey-Vargas, R., Frey, F. A. & López-Escobar, L. (1991). Recent lavas from the Andean volcanic front (33 to 42°S); Interpretations of along-arc compositional variations. In: Harmon, R. S. & Rapela, C. W. (eds) *Andean Magmatism and its Tectonic Setting. Geological Society of America, Special Papers* **265**, 57–77.

Valencio, S. A., Ramos, A. M., Cagnoni, M. C., Panarello, H. O., Cabaleri, N. G. & Armella, C. (2003). Isotope signal of the middle Jurassic carbonate ramp of Calabozo Formation, at Arroyo El Plomo, Mendoza, Argentina. In: Sial, A. N., Chemale, Jr, F., McReath, I., Bettencout, J. S., Pimentel, M. M. & Macambira, M. J. B. (eds) *Short Papers of the IV South American Symposium on Isotope Geology.* Salvador, pp. 409–412.

Van Benthem, S., Govers, R., Spakman, W. & Wortel, M. J. R. (2013). Tectonic evolution and mantle structure of the Caribbean. *Journal of Geophysical Research: Solid Earth* **118(6)**, 3019–3036.

van der Meer, D. G., Spakman, W., van Hinsbergen, D. J. J., Amaru, M. L. & Torsvik, T. H. (2010). Towards absolute plate motions constrained by lower-mantle slab remnants. *Nature Geoscience* **3(1)**, 36–40.

van der Meer, D. G., Torsvik, T. H., Spakman, W., van Hinsbergen, D. J. J. & Amaru, M. L. (2012). Intra-Panthalassa Ocean subduction revealed by fossil arcs and mantle structure. *Nature Geoscience* **5**, 215–219.

Villemant, B. (1988). Trace-element evolution in the Phlegrean Fields (Central Italy)—Fractional crystallization and selective enrichment. *Contributions to Mineralogy and Petrology* **98(2)**, 169–183.

Villemant, B., Jaffrezic, H., Joron, J. L. & Treull, M. (1981). Distribution coefficients of major and trace-elements: Fractional crystallization in the alkali basalt series of Chaîne-Des-Puys (Massif Central, France). *Geochimica et Cosmochimica Acta* **45(11)**, 1997–2016.

Wagner, L. S., Beck, S. & Zandt, G. (2005). Upper mantle structure in the south central Chilean subduction zone (30° to 36°S). *Journal of Geophysical Research* **110**, B01308.

Watson, E. B. & Green, T. H. (1981). Apatite/liquid partition coefficients for the rare earth elements and strontium. *Earth and Planetary Science Letters* **56**, 405–421.

Weaver, S. D., Gibson, I. L., Houghton, B. F. & Wilson, C. J. N. (1990). Mobility of rare earth and other elements during crystallization of peralkaline silicic lavas. *Journal of Volcanology and Geothermal Research* **43**, 57–70.

Yuan, X., Asch, G., Bataille, K., Bock, G. & Bohm, N. (2006). Deep seismic images of the Southern Andes. In: Kay, S. M. & Ramos, V. A. (eds) *Evolution of an Andean Margin: A Tectonic and Magmatic View from the Andes to the Neuquén Basin (35°–39°S lat). Geological Society of America, Special Papers* **407**, 61–72.

Zindler, A. & Hart, S. (1986). Chemical geodynamics. *Annual Review of Earth and Planetary Sciences* **14**, 493–571.